eLife

Reviewed Preprint
v1 • April 14, 2026
Not revised

For correspondence:
mmellado@cnb.csic.es

Competing interests: JMP has received research funding, consultancy fees, and lecture sponsorships from and has served on advisory boards for various companies (AbiVax, AstraZeneca, MSD, Gilead Sciences, ViiV Healthcare, Johnson & Johnson) outside the scope of this article. The rest of the authors declare no competing interests.

Funding: See page 22

Reviewing editor: Laura Ruth Delgui, Consejo Nacional de Investigaciones Científicas y Técnicas, Argentina



# HIV-1 Envelope glycoprotein modulates CXCR4 clustering and dynamics on the T cell membrane

**Adriana Quijada-Freire[1], César A Santiago[2], Eva M García-Cuesta[1], Blanca Soler-Palacios[1], Rosa Ayala-Bueno[1], Sofía R Gardeta[1], Enara San Sebastian[3], Eva Armendariz-Burgoa[4], María C Puertas[4], Ricardo Villares[1], Urtzi Garaigorta[3], Luis Ignacio González-Granado[5,6], José Miguel Rodríguez-Frade[1], Jakub Chojnacki[4,7,8], Javier Martinez-Picado[4,7,9,10], Mario Mellado[1]**

[1]Chemokine Signaling group, Department of Immunology and Oncology, Centro Nacional de Biotecnología/CSIC, Campus de Cantoblanco, Madrid, Spain • [2]X-ray Crystallography Unit, Department of Macromolecules Structure, Centro Nacional de Biotecnología/CSIC, Campus de Cantoblanco, Madrid, Spain • [3]Departamento de Biología Molecular y Celular, Centro Nacional de Biotecnología/CSIC, Campus de Cantoblanco, Madrid, Spain • [4]IrsiCaixa, Badalona, Spain • [5]12 de Octubre Health Research Institute (imas12), Madrid, Spain • [6]Department of Public Health School of Medicine, School of Medicine, Universidad Complutense de Madrid, Madrid, Spain • [7]CIBERINFEC, Madrid, Spain • [8]Germans Trias i Pujol Research Institute (IGTP), Badalona, Spain • [9]University of Vic-Central University of Catalonia, Vic, Spain • [10]Catalan Institution for Research and Advanced Studies (ICREA), Barcelona, Spain

## eLife Assessment

This study provides **valuable** insights into how HIV-1 Env modulates the nanoscale organization and dynamics of the CXCR4 co-receptor on T cells, using quantitative imaging and functional approaches, the authors present **convincing** evidence that gp120 engagement promotes CD4-dependent clustering and altered mobility of CXCR4, distinct from the effects of the natural ligand CXCL12. Some concerns were raised regarding the interpretation of the single-particle tracking analyses, and additional clarification or analysis may help strengthen the conclusions. The physiological relevance of the findings could be further enhanced by validation with infectious virus and by more clearly integrating the CXCR4R334X mutant observations into the central mechanistic narrative. The work will be of interest to researchers studying HIV entry and membrane receptor organization.

[Editors' note: this paper was reviewed by *Review Commons*.]

https://doi.org/10.7554/eLife.110354.1.sa5

## Abstract

HIV-1 entry into susceptible cells requires the dynamic interaction of its envelope (Env) glycoprotein with the host cell receptor CD4 and a co-receptor, either CCR5 or CXCR4. While the core molecular mechanisms driving Env-receptor interactions and subsequent membrane fusion are well characterized, the precise nanoscale spatial reorganization of these co-receptors at the viral binding site remains poorly defined. In this study, we employed single-particle tracking total internal reflection fluorescence (SPT-TIRF) microscopy to quantitatively analyze nanoscale organizational changes of CXCR4 on the surface of $CD4^+$ T cells following binding by X4-tropic HIV-1. Our data reveal that both recombinant X4-gp120 and virus-like particles expressing physiological levels of X4 Env proteins (gp120 and gp41) promote CXCR4 clustering, a phenomenon linked to cell infection. Furthermore, these ligands induced oligomerization of $CXCR4^{R334X}$, a naturally occurring mutant associated with WHIM syndrome that supports HIV-1 infection but fails to oligomerize in response to CXCL12. Our findings establish a link between CXCR4 clustering

and HIV-1 infection, enhancing our understanding of the initial events in viral attachment and entry. These results further suggest that HIV-1 depends on a specific spatial arrangement of co-receptors, distinct from that induced by their natural chemokine ligands, highlighting the critical role of cell-surface receptor spatial organization in dictating cellular function.

# Introduction

HIV-1 infects immune cells through a dynamic interaction between its envelope glycoprotein complex (Env), composed of gp41 and gp120 trimers (1, 2), and two receptors on target cells: the primary receptor CD4, and a co-receptor, either CCR5 or CXCR4. These co-receptors are critical for viral entry and determine viral tropism. R5 strains (M-tropic) infect primary macrophages and certain memory $CD4^+$ T cells by binding to CD4 and CCR5(3), while X4 strains (T-tropic) infect primary $CD4^+$ T cells by binding to CD4 and CXCR4 (4).

R5-tropic viruses are typically the primary mode of transmission in humans and remain prevalent throughout the infection (5). However, in many infected individuals, the virus evolves its tropism over time, progressing from R5-tropic to dual-tropic (R5/X4), and ultimately to X4-tropic as the infection advances (6). This shift in tropism is associated with a more rapid decline in $CD4^+$ T cell counts (7). Furthermore, CXCR4 has been implicated in the infection of hematopoietic progenitor cells, potentially contributing to the establishment of long-lasting latent HIV-1 reservoirs (8).

The fusion of viral and cellular membranes is initiated by the binding of gp120 to CD4 (9, 10), which triggers a conformational change in gp120 that facilitates co-receptor engagement (11). These structural changes expose the N-terminal hydrophobic fusion peptide of gp41, which inserts into the cell membrane (12) to establish a fusion pore and release the viral contents into the target cell.

Numerous structural and biophysical studies have examined the HIV-1 infection process, successfully clarifying the structural requirements and conformational changes in gp120 and gp41 that enable membrane fusion and viral entry (13–16). Early investigations into host cell components revealed that HIV-1 infection induces the redistribution of cell-surface CD4 and co-receptors to the sites of viral attachment (17, 18). More recent evidence, obtained through super-resolution microscopy, demonstrates that HIV-1 binding triggers CD4 clustering, a phenomenon also observed (albeit to a lesser degree) following stimulation with gp120 alone (19). However, less is known about which specific co-receptors are also recruited to the virus particles bound to the cell surface. It is known that gp120 can mediate the association of CD4 with both CXCR4 and CCR5 (17, 20, 21). Furthermore, it has been shown that the co-expression of CCR5 modifies the conformation of both CXCR4 homodimers and CD4/CXCR4 heterodimers. This conformational change prevents the binding of gp120 from an X4 HIV-1 strain, specifically $gp120_{IIIB}$, to the resulting CD4/CXCR4/CCR5 complex (22).

Large-scale molecular assemblies at the cell membrane, often termed signaling clusters or nanoclusters, are increasingly recognized as key regulators of cell signaling (23). Evidence indicates that the spatial reorganization and distribution of membrane receptors are key to controlling cell functions. Notably, clustering also appears to be essential for viral infection. For instance, Env–CD4 complexes form clusters and ring-like structures, facilitating closer contact between opposing membranes (24). These clusters often govern a significant portion of the overall signaling process and are frequently associated with the cytoskeleton (23). For example, CD4 receptors exist in pre-clustered structures that enlarge upon T cell activation, thereby modulating the strength of the signaling response (25, 26). Moreover, CXCR4 is organized at the cell membrane as monomers, dimers and small aggregates (groups of ≥3 receptors) called nanoclusters. The binding of its specific ligand, CXCL12, leads to a decrease in the proportion of monomers/dimers, while simultaneously increasing the formation of larger nanoclusters. This change in receptor organization consequently alters the lateral mobility of CXCR4 within the cell membrane (27). This mechanism is critical for initiating CXCR4 signaling and enabling cells to accurately orient themselves in response to CXCL12 gradients (28). A naturally occurring CXCR4 mutant,

CXCR4$^{R334X}$, which is responsible for WHIM syndrome, a severe immunological disorder (29), fails to form these large nanoclusters upon CXCL12 binding. Consequently, cells carrying this mutation lose their ability to properly sense chemoattractant gradients (28).

Here, we employed quantitative single-particle tracking in total internal reflection fluorescence (SPT-TIRF) microscopy to directly investigate the spatial arrangement and dynamic activity of CXCR4 upon exposure to HIV-1 glycoproteins. Our findings reveal that both recombinant X4-gp120 and virus-like particles (VLPs) containing a limited number of X4 Env proteins (gp120 and gp41) promote CXCR4 clustering on cells expressing CD4 and CXCR4. Moreover, they trigger the oligomerization of CXCR4$^{R334X}$. These results suggest that, along with CD4 clustering, the conformational changes in chemokine receptors triggered by HIV-1 are essential for cell infection and differ from the effects of the natural ligand, CXCL12. Therefore, CD4/CXCR4 complexes and their interaction sites represent potentially valuable targets for developing novel therapeutic strategies to block HIV-1 entry.

# Materials and methods

## Cells and reagents

HEK-293T cells, Jurkat human leukemia cells (JKCD4$^-$X4$^+$), and Daudi cells were obtained from the American Type Culture Collection (CRL-3216, CRL-10915 and CCL-213, respectively; ATCC, Rockville, MD). HEK-293CD4 cells, Jurkat CD4$^+$ cells (JKCD4$^+$X4$^+$), and Jurkat cells expressing an X4-tropic HIV-1 Env (JKHXBC2) were kindly provided by Drs. G. del Real (Instituto Nacional de Investigación y Tecnología Agraria y Alimentaria, Madrid, Spain) and J. Alcamí (Centro Nacional de Microbiología, Instituto de Salud Carlos III, Madrid, Spain). Where indicated, Jurkat cells lacking endogenous *CXCR4* (JKCD4$^+$X4$^-$) (30) were electroporated with plasmids expressing wild-type CXCR4-AcGFP or mutant CXCR4$^{R334X}$-AcGFP receptors (20 μg), as described (30). Stable Jurkat cells expressing CXCR4$^{R334X}$ (JKCD4$^+$CXCR4$^{R334X}$) were generated by electroporation with CXCR4$^{R334X}$ and antibiotic selection (30).

Human peripheral blood mononuclear cells (PBMCs) were isolated from the blood of a patient with WHIM syndrome (CXCR4$^{R334X}$) or from healthy donors, and when required from buffy coats of healthy donors, which were obtained from the Centro de Transfusiones (Comunidad Autónoma de Madrid, Spain) by centrifugation through Percoll density gradients (760 × g, 45 min, room temperature [RT]). CD4$^+$ cells were purified by negative selection using Dynabeads (Invitrogen, Thermo Fisher Scientific, Waltham, MA) and activated *in vitro* for 1 week with 50 U/mL of IL-2 (Teceleukin; Roche, Nutley, NJ) and 5 μg/mL phytohemagglutinin (Roche, Basel, Switzerland) to generate T cell blasts (31). The study using blood from WHIM patients and healthy donors was approved by the Institutional Review Board of the 12 de Octubre Health Research Institute (N° CEIm: 24/248), and was conducted according to the principles of the Declaration of Helsinki. Informed consent was obtained from all patients.

Recombinant gp120 protein, HXBc2, was obtained from MyBiosource (#MBS43404, MyBiosource Inc., San Diego, CA). The following antibodies were used: anti-human CXCR4 monoclonal antibody (mAb) (clone 44717) and phycoerythrin-conjugated anti-human CXCR4 mAb (clone 12G5; both from R&D Systems, Minneapolis, MN); goat F(ab')2 anti-mouse IgG-PE (Southern Biotech, Birmingham, AL); anti-human CD4 mAb (clone OKT4; Biolegend, San Diego, CA); anti-histidine mAb (clone AD1.1.10; R&D Systems); rabbit anti-gp120$_{IIIb}$ Ab (32); rabbit anti-Gag p24 HIV-1 mAb (R&D Systems); and anti-phospho-AKT mAb (S473; #4060), anti-phospho-ERK1,2 mAb (T202/Y204; #9191), and anti-phospho-Lck mAb (Y505; #2751) (all from Cell Signaling Technology, Danvers, MA); anti-tubulin mAb conjugated with rhodamine (Bio-Rad, Hercules, CA); phalloidin-TRITC (#P1951, Sigma-Merck, St Louis, MO); anti-ICAM 3 mAb (clone HP2/19) kindly donated by Dr. Francisco Sánchez Madrid (Instituto Sanitario Hospital Universitario La Princesa); goat anti-mouse-AF488 Ab (Thermo Fisher Scientific); anti-human gp120 mAb Fab fragments (clone 2G12; Polymun Scientific, Vienna, Austria); anti-human IgG Fab fragments (Jackson ImmunoResearch, West Grove, PA) conjugated to Abberior STAR RED (Abberior GmbH, Gottingen, Germany), kindly donated by Dr. Jakub Chojnacki (Germans Trias i Pujol Research Institute (IGTP)); anti-p24 HIV-1

(clone 37G12; Polymun Scientific) conjugated with Abberior STAR ORANGE. Human CXCL12 was obtained from PeproTech (Rocky Hill, NJ), and human CXCR4 was cloned into the pAcGFPm-N1 plasmid (Clontech Laboratories, Palo Alto, CA), as described (33).

Fab fragments for staining in stimulated emission depletion (STED) microscopy were generated from the respective IgGs using the Fab Micro Preparation 3 Kit (Pierce, Thermo Fisher Scientific). The quality of Fab preparations was determined by measuring the absorbance of the eluted fractions of each conjugated antibody (at 280 nm and at the wavelength of maximum absorption of the fluorochrome). Anti-human Fab fragments were coupled to Abberior STAR RED dye *via* NHS-ester chemistry according to the dye manufacturer's instructions.

CellTracker Orange CMTMR and Blue CMAC (#C2927 and #C2110, respectively) were from Thermo Fisher Scientific.

## Gene constructs

Genes of HIV-1 gp120 (residues 31-507) from the isolate HXB2 (HIV-$1_{IIIB}$), with a C-terminal 6×histidine tag, were amplified by PCR from pHXB2-env (#1069 NIH-AIDS Reagent Program) using the oligonucleotides 5'NheI (5' TAACCGGTGCCAC CATGGACAGAGCCAAGCTGCTGCTGTTGCTGCTGCT GCTGCTGCTGCCTCAG GCTCAGGCCACTGAGAAGCTGTGGGTG 3') and 3'NotI (5' ATGCGGCCGCTCA GT GATGGTGATGGTGATGGGATCCACGCGGAACCAGCTGCACCACTCTTCT 3'), and were cloned into pIRES-PURO3 (#631619 from Clontech Laboratories).

The CD4 extracellular domain (residues 1-388), with a C-terminal 6×histidine tag, was amplified by PCR from CD4-pcDNA-3.1, kindly donated by Dr. Santos Mañes (Centro Nacional de Biotecnología, CSIC) (34) using the oligonucleotides 5'AgeI (5' TAACCGGTATGAACCGGGGAGTCCCT 3') and 3' NotI (5' ATGCGGCCGCCTAGTATG GTGATGGTGATGCAAGTCCTCTTCAGAAATGAGCTTTTGCTCGGGCAGAAC CTTGAT 3'), and was cloned into pIRES-PURO3 (#631619 from Clontech Laboratories). Stably-transfected HEK-293T cell lines were generated for each construct. Briefly, $0.5 \times 10^6$ cells were seeded in DMEM supplemented with 10% FCS in a 6-well plate 24 hours before transfection. Cells were then transfected with Expifectamine in OptiMem media (ExpiFectamine™ 293 transfection kit; #A14525 from Thermo Fisher Scientific). At 48 hours post-transfection, cells were transferred to DMEM containing 10% FBS and 2μg/mL puromycin for selection ($1 \times 10^4$ cells per well in a 96-well plate). Protein expression was confirmed by western blotting (using anti-gp120IIIB or anti-histidine mAbs, depending on the construct). Positive clones were expanded, frozen, and stored in liquid nitrogen.

## Purification of recombinant proteins: soluble HIV-1 gp120 and soluble CD4

HEK-293T cells expressing C-terminal his-tagged HXB2-gp120 or the extracellular CD4 domain were grown in DMEM containing 10% FBS and 2 μg/mL puromycin in 150-mm plates. The filtered supernatants were passed through a Nickel Agarose Extrachel column, Ni-NTA, (ABT technologies, Madrid, Spain) at a flow rate of 0.5 mL/min. Each recombinant histidine-tagged protein was eluted utilizing a step-gradient protocol using a Tris 50 mM pH 8, NaCl 500 mM buffer containing 500 mM imidazole. The elution involved initial steps of 10% and 20% imidazole, followed by a linear gradient to 100% to ensure complete protein recovery. The eluted fractions were analyzed by SDS-PAGE gel electrophoresis. Those fractions containing the protein of interest were pooled and concentrated to a final volume of 0.5 mL. The concentrated sample was subjected to gel filtration chromatography using a S200 Increase (10/300) column (Cytiva, Freiburg, Germany). The eluted fractions were analyzed by SDS-PAGE and fractions containing the expected molecular size were pooled, aliquoted, and stored at −80°C.

## Production of viral-like particles and lentiviral particles

Production of VLPs in HEK-293T cells included transfection with a plasmid encoding the X4-tropic HIV-1 Env (10 μg pHXB2env; #1069 NIH-AIDS Reagent Program) and a plasmid encoding a second-generation packaging system (7 μg psPAX2; #12260 Addgene, Watertown, MA). Supernatants were

collected 48 hours post-transfection, filtered through 0.45 µm filters, and clarified by ultracentrifugation (247,000 × g, 2 h, 4°C) on a 20% sucrose cushion, using a Beckman SW55 rotor. The resulting VLPs were aliquoted and stored at −80°C. Expression of gp120 and p24 was assessed by western blotting with specific antibodies. Each VLP batch was quantified using a p24 Quantikine ELISA kit (R&D Systems).

Production of lentiviral particles (LVPs) was performed as above with the co-transfection of a reporter gene (8 µg plGFP; #PS100065, OriGene, Rockville, MD) instead of the double transfection. Supernatants were collected 48 hours post-transfection, filtered through 0.45 µm filters, aliquoted, and stored at −80°C. Expression of gp120 and p24 was assessed by western blotting with specific antibodies. Each LVP batch was characterized in a transduction assay using LVPs transfected with the vesicular stomatitis virus G glycoprotein (VSVG) (pCMV-VSV-G; #8454, Addgene) as a positive control.

## Western blotting

Cells ($3 \times 10^6$) were activated with CXCL12 (50 nM) or recombinant X4-gp120 (0.3 µg/mL) at the time points indicated and then lysed in RIPA detergent buffer containing 1 mM PMSF, 10 µg/mL aprotinin, 10 µg/mL leupeptin, and 10 µM sodium orthovanadate (30 min, 4°C). Cell extracts were analyzed by western blotting using specific antibodies. Densitometric evaluation of western blots was performed using ImageJ software (NIH, Bethesda, MD).

## Flow cytometry

Cells ($2 \times 10^5$/well) were incubated with specific antibodies (30 min, 4°C) and mean fluorescence intensity (MFI) was determined on a Gallios or FC500 flow cytometer (Beckman Coulter). When required, Jurkat cells expressing CD4 (JKCD4$^+$X4$^+$ and JKCD4$^+$X4$^-$) were incubated with X4-gp120-His (0.3 µg/mL), followed by staining with an anti-histidine-PE mAb. Similarly, Daudi cells were incubated with a mixture of X4-gp120 (0.3 µg/ml) and soluble hCD4-his (0.2 µg/mL), and subsequently stained with an anti-histidine-PE mAb.

For human PBMCs, 100 µL of whole blood from healthy controls and a WHIM patient were analyzed by flow cytometry for the expression of CD3-APC (IM2467), CD19-PC5.5 (A66328), CD4-FITC (A07750), CD8-PC7 (737661; all from Beckman Coulter Inc., Brea, CA), and CXCR4-PE (306506, Biolegend) using a Gallios flow cytometer and FlowJo software. Receptor internalization was evaluated after cell activation ($5 \times 10^5$ cells/well) with 50 nM CXCL12 or 0.3 µg/mL of recombinant X4-gp120 at the indicated time points. Cells were incubated with an anti-CXCR4 mAb (clone 44717, 30 min, 4°C), followed by a PE-coupled goat anti-mouse IgG (30 min, 4°C) or, when required, with anti-CD4 (clone OKT4, 20 min, 4°C), and analyzed in a Cytoflex cytometer (Beckman Coulter). Results are expressed as a percentage of mean spot intensity (MSI) of treated cells relative to that of unstimulated cells.

To evaluate VLPs by flow cytometry, particles were coupled to latex beads (4 mm, 4% w/v Aldehyde/Sulfate latex; Invitrogen, Eugene, OR). After sonication (5 min, RT), beads were mixed with VLPs at a ratio of 1:1 v/v (15 min, RT) in 1% casein-PBS solution (Bio-Rad). Reactive groups were blocked with 100 mM glycine (60 min, 4°C, with continuous rocking). Beads coupled to VLPs were washed twice by centrifugation (3 min, 2000 × g) in washing buffer (PBS/BSA 0.5%), resuspended, and incubated with the corresponding dilution of the recombinant soluble CD4 in casein-PBS solution (30 min, RT). VLP-beads conjugates were washed three times (3 min, 2,000 × g) with PBS staining buffer (PBS supplemented with 2% FBS, 1% BSA, and 0.2% sodium azide) and stained as above for flow cytometry.

## Lentiviral particle transduction assays

HEK-293 CD4 cells ($1.2 \times 10^4$ cells per well in a 96-well plate) were inoculated with serial dilutions of LVP-containing supernatants. Stock solutions were diluted in DMEM, 10% FCS, 1 mM pyruvate, and 2 mM glutamine. Sixteen hours later, the viral inoculum was replaced with fresh medium and the cells were further incubated (48 h, 37°C). Viral transduction efficiency was determined by GFP fluorescence analysis. The medium was discarded and cells were washed with PBS and fixed using

4% formaldehyde in PBS (20 min, RT). Fluorescence was imaged in a Tecan Spark Cyto plate reader (Tecan Group Ltd., Männedorf, Switzerland) after extensive washes with PBS. Images of 2456 × 2052 pixels at a 16-bit gray scale were acquired with a 4× objective. All images were captured using identical exposure settings (200 ms), except for wells where cells were transduced with LVPs expressing VSVG, for which an exposure time of 80 ms was used. Mean fluorescence intensity of GFP signal of each image was quantitated using Fiji/ImageJ v2.3.0/1.53t software.

## Cell-cell fusion assay

The JKHXBC2 cell line was co-cultured with the indicated Jurkat target cells at a 1:1 ratio in 96-well flat-bottom plates (16 h, 37°C). Prior to co-culture, each cell type was stained with vital probes CellTracker Orange CMTMR and Blue CMAC, respectively. Double-stained events were subsequently analyzed using a Gallios Analyzer cytometer (Beckman Coulter). Results are shown as the percentage of fusion events ± SD, using as a reference the fusions events detected in JKCD4$^+$CXCR4$^+$ cells.

## Cell adhesion/migration on planar lipid bilayers

Planar lipid bilayers were prepared as reported (35). Briefly, unlabeled GPI-linked intercellular adhesion molecule 1 (ICAM-1) liposomes were mixed with 1,2-dioleoyl-phosphatidylcoline. Membranes were assembled in FCS2 chambers (Bioptechs, Butler, PA), blocked with PBS containing 2% FCS (60 min, RT), and coated with CXCL12 (200 nM, 30 min, RT) or gp120 (0.3 µg/ml, 30 min, RT). Cells ($3 \times 10^6$ CD4$^+$ T blasts/mL) in PBS containing 0.5% FCS, 0.5 g/L D-glucose, 2 mM $MgCl_2$, and 0.5 mM $CaCl_2$ were then injected into the pre-warmed chamber (37°C). Confocal fluorescence, differential interference contrast (DIC) and interference reflection microscopy (IRM) images were acquired on a Zeiss Axiovert LSM 510-META inverted microscope with a 40× oil-immersion objective. Imaris 7.0 software (Bitplane, Zurich, Switzerland) and ImageJ 1.49v were used for qualitative and quantitative analysis of cell dynamics parameters, fluorescence and IRM signals. The fluorescence signal of the planar bilayer in each case was established as the background fluorescence intensity. The frequency of adhesion (IRM$^+$ cells) per image field was estimated as [n° of cells showing IRM contact/total number of cells (estimated by DIC)] × 100; similarly, we calculated the frequency

## STED assays

Purified particles (~1 µg of p24) were adhered to glass cover slips previously coated with 0.01% poly-L-lysine (Sigma) for 20 minutes. Cover slips were briefly fixed with 3% PFA/PBS and blocked using 2% BSA (Sigma)/PBS for 30 minutes. Particles were stained for Env using 10 ng/µL 2G12 Fab fragments and anti-human Abberior STAR RED- conjugated Fab fragments. Following immunostaining, particles were washed in permeabilization buffer (0.1% saponin, 0.5% BSA in PBS) and stained for Gag using 20 ng/µL 37G12 Ab conjugated with STAR ORANGE. The samples were briefly fixed using 3% PFA/PBS again and were overlaid with SlowFade Diamond (Thermo Fisher Scientific). All steps were carried out at RT.

The VLPs were imaged using an Olympus IX83 inverted confocal microscope equipped with the Abberior STEDYCON STED system using a 60×/1.42NA objective. The following parameters were used during STED image acquisitions: pinhole size: 1 Airy; dwell time: 300 µs/pixel; field of view: 20 µm × 20 µm and pixel size: 20 nm. The mature state of VLPs, the percentage which express gp120 on their surface and the intensity of the signal of gp120 per VLP, were quantified manually using ImageJ.

## Imaging of viral-like particles by transmission electron microscopy

The integrity of VLPs was examined by negative-stain electron microscopy on carbon grids. Samples were incubated on the grids and were treated with 2% uranyl acetate (30 s, RT). Grids were examined using a transmission electron microscope (1200-EX II; Jeol, Tokyo, Japan) at 100 kV, equipped with a Gatan Oneview CMOS camera.

## FRET saturation curves by sensitized emission

FRET analyses were performed as described (36). Briefly, HEK-293T cells ($3.5 \times 10^5$ cells/well) were transiently transfected with cDNA encoding the fusion proteins using the poly-ethylenimine method (Sigma-Aldrich). For CD4/CXCR4 or CD4/$CXCR4^{R334X}$ heterodimers, the cells were co-transfected with a fixed amount of CD4-CFP (2 µg) and increasing amounts of CXCR4-YFP or $CXCR4^{R334X}$-YFP (0.5–8.0 µg). As a control, we used a fixed amount of CD4-CFP (2 µg) and increasing amounts of $5HT_{2B}$-YFP (0.5–12 µg). We incubated cells with cDNA and poly-ethylenimine (5.47 mM in nitrogen residues) and 150 mM NaCl in serum-free medium, which was replaced after 4 hours by complete medium. At 48 hours post transfection, cells were washed twice in HBSS supplemented with 0.1% glucose and resuspended in the same solution. Total protein concentration was determined for whole cells using the Bradford Assay Kit (Bio-Rad). Cell suspensions (0.2 µg/µL) were added to black 96-well microplates and emission light was quantified using the Wallac Envision 2104 Multilabel Reader (Perkin-Elmer, Waltham, MA) as described (27). To determine $FRET_{50}$ and $FRET_{max}$ values, curves were extrapolated from data using a nonlinear regression equation applied to a single binding site model with a 95% confidence interval (GraphPad PRISM software, San Diego, CA). When FRET at a fixed ratio was needed, HEK-293T cells were transiently co-transfected with a fixed ratio of CXCR4-YFP/CD4-CFP (15 µg and 9 µg, respectively) and $CXCR4^{R334X}$-YFP/CD4-CFP (9 µg and 9 µg, respectively in all cases). After 48 hours the cells were treated with Env(-) VLPs (0.1 µg/mL of Gag p24) or gp120-VLPs (0.1 µg/mL of Gag p24) and FRET efficiency was evaluated (n = 3, mean ± SD).

## Single-molecule TIRF imaging and analysis

Transfected cells expressing 8,500–22,000 receptors/cell (<4.5 particles/$\mu m^2$) were selected for detection and tracking analysis. Experiments were performed at 37°C with 5% $CO_2$ using a TIRF microscope (Leica AM TIRF inverted microscope; Leica Microsystems, Wetzlar, Germany). Image sequences of individual particles (500 frames) were then acquired at 49% laser power (488-nm diode laser) with a frame rate of 10 Hz (100 ms/frame). The penetration depth of the evanescent field was 90 nm. Particles were detected and tracked using the U-Track2 algorithm (37) implemented in MATLAB, as described (27). MSI, number of mobile and immobile particles and diffusion coefficients ($D_{1\text{-}4}$) were calculated from the analysis of thousands of single trajectories over multiple cells (statistics provided in the respective figure captions) using described routines (27). The receptor number along individual trajectories was determined as reported (38), using the intensity of the monomeric protein CD86-AcGFP as a reference (Supplementary Figure 1). Values were confirmed using single-step photobleaching analysis (27, 28).

## HIV-1 infection in T $CD4^+$ cells of a WHIM patient

All donors were female and under the age of 30. PBMCs were obtained from sero- negative fresh blood of a WHIM patient and three healthy donor controls using SepMate tubes (STEMCELL Technologies, Vancouver, Canada). Isolated PBMCs were cultured in RPMI supplemented with 20% FBS (Gibco), 1% penicillin/streptomycin (Capricorn Scientific GmbH, Ebsdorfergrund, Germany), 3 µg/mL PHA (Sigma-Aldrich), and 10 U/mL of IL-2 (Novartis, Basel, Switzerland) for 48 hours at 37°C. Activated PBMCs were inoculated *in vitro* at a multiplicity of infection (MOI) of 0.001 with the HIV-1 NL4- 3 lab strain for 1 hour. After removal of the viral inoculum, cultures were split into two wells and maintained in RPMI supplemented with 20% FBS, 1% penicillin/streptomycin, and 10 U/mL of IL-2. Supernatants were collected at different time points and replaced with fresh supplemented media. The infection rate was determined by quantification of viral p24 in the supernatants using the Alliance HIV-1 p24 Antigen Elisa Kit (Perkin Elmer).

## Statistical analyses

All results were analyzed with GraphPad Prism software version 9. Cell polarization assays, using immunofluorescence or planar lipid bilayers comparing different conditions, were analyzed to determine significant differences between means using one-way analysis of variance (ANOVA)

followed by Tukey's multiple comparisons test. Data related to the percentage of mature VLPs and their surface expression of gp120 obtained by STED microscopy, and MFI results by flow cytometry, were also analyzed by one-way ANOVA and Tukey's multiple comparisons test. A two-tailed Mann-Whitney non-parametric test was used to analyze the MFI of gp120 per VLP. The Kruskal-Wallis test followed by Dunn's test was used to analyze MSI and diffusion coefficients ($D_{1-4}$) of single particles in TIRF experiments. We used contingency tables to compare two or more groups of categorical variables, such as the percentages of mobile or immobile particles, and these were compared using a Chi-square test with a two-tailed p-value. Statistical differences were reported as n.s. = not significant $p > 0.05$, *$p \leq 0.05$, **$p \leq 0.01$, ***$p \leq 0.001$ and ****$p \leq 0.0001$.

# Results

## Recombinant gp120-mediated CXCR4 clustering requires CD4 expression

To evaluate the role of HIV-1 in modulating CXCR4 dynamics at the cell membrane, we first synthesized a recombinant X4 HIV-1 gp120 (X4-gp120) with a C-terminal histidine tag to facilitate subsequent detection. We generated a HEK-293T cell line that constitutively secretes the recombinant glycoprotein. The secreted X4-gp120 was isolated from cell culture supernatants using a simple, rapid, non-denaturing and efficient purification procedure involving Ni-NTA agarose chromatography and gel filtration chromatography. The purity of the isolated glycoprotein was confirmed by SDS-PAGE and western blotting, using commercial gp120 as a control and specific antibodies (Supplementary Figure 2A, B). The X4-gp120 specifically bound to Jurkat cells expressing CD4, regardless of the presence or absence of CXCR4 (JKCD4$^+$CXCR4$^+$ and JKCD4$^+$CXCR4$^-$, respectively) (Supplementary Figure 2C). By contrast, X4-gp120 did not bind to Daudi cells, which express only CXCR4 (Supplementary Figure 2D). In this latter case, X4-gp120 binding became possible when the recombinant protein was pre-incubated with soluble CD4. As a control, no binding of soluble CD4 was detected in the absence of X4-gp120 (Supplementary Figure 2D). These data indicate that our recombinant gp120 is a X4-tropic gp120 capable of binding Jurkat cells expressing CD4.

Engagement of the HIV-1 Env with CD4 and/or a chemokine co-receptor activates several signal transduction pathways (39, 40). For instance, gp120 binding to CD4 leads to the phosphorylation of the receptor tyrosine kinase p56Lck, which then activates the Raf/MEK/ERK and phosphatidylinositol 3-kinase (PI3K) pathways (41). PI3K is also activated through chemokine receptor engagement (42), and only viruses capable of inducing signaling *via* these receptors can establish productive infections (40). Jurkat cells and primary CD4$^+$ T blasts were stimulated with X4-gp120, then lysed and analyzed by western blotting. The results showed that Akt, ERK1/2 and Lck were rapidly phosphorylated following X4-gp120 activation (Supplementary Figure 3A, B) in both cell types. Furthermore, it is known that the interaction of gp120 with CXCR4 influences the actin cytoskeleton (43). Cytochalasin D, an inhibitor of F-actin polymerization, has been shown to inhibit viral entry into PBMCs (44), and to affect the formation of HIV-1 reverse transcriptase products in HeLa cells (45). We thus evaluated whether X4-gp120 reorganized the actin cytoskeleton of the target cells. Using artificial lipid bilayers coated with ICAM-1, we observed that both CXCL12 and X4-gp120 induced the polarization of primary CD4$^+$ T blasts and, furthermore, enhanced cell adhesion (Supplementary Figure 4A, B). However, only CXCL12 triggered significant cell migration (Supplementary Figure 4C). These findings confirmed that X4-gp120 bound CXCR4 in the presence of CD4 and was fully functional on both primary CD4$^+$ T blasts and Jurkat cells.

The actin cytoskeleton acts as a physical barrier, influencing the compartmentalization of the plasma membrane and the dynamics of membrane proteins (46, 47). Consequently, the dynamic nature of actin not only defines cell shape during migration, but also affects membrane organization of both CD4 (48) and CXCR4 (27). Next, we transiently transfected JKCD4$^+$X4$^-$ cells, which express endogenous CD4, with CXCR4-AcGFP. We then used SPT in TIRF-M mode to observe individual molecules within the plasma membrane, allowing us to determine the effect of X4-

gp120 on CXCR4 dynamics and stoichiometry (Supplementary video 1-3). Consistent with previous observations (27, 28), our analysis of CXCR4 dynamics in unstimulated cells revealed that the majority of CXCR4 particles were mobile (~87%) (Figure 1A), exhibiting a median short time-lag diffusion coefficient ($D_{1-4}$) of 0.017 $\mu m^2 s^{-1}$ (Figure 1B). Upon stimulation, both CXCL12 and X4-gp120 significantly reduced the overall receptor diffusivity (CXCL12, median $D_{1-4}$ = 0.007 $\mu m^2 s^{-1}$; X4-gp120, median $D_{1-4}$ = 0.009 $\mu m^2 s^{-1}$) (Figure 1B), and increased the percentage of immobile particles from ~13% (basal) to ~20% (CXCL12), and to ~18% (X4-gp120) (Figure 1A). Mobile particles exhibited distinct diffusion profiles, derived from mean square displacement (MSD) plots (49), and were further classified based on motion using the moment scaling spectrum (50). For most mobile particles (~90% in unstimulated cells, ~79% in CXCL12-activated cells, and ~75% in X4-gp120 stimulated cells), diffusion was confined (Supplementary Figure 5A). To quantify the number of receptors in individual trajectories, we measured the average fluorescence intensity during the initial 20 frames of each trajectory and used the intensity of the monomeric protein CD86-AcGFP as a reference (28, 51) (Supplementary Figure 1). In unstimulated cells, we found a predominance of CXCR4 monomers and dimers (~98%), with only a minor fraction of oligomers, complexes containing more than three receptors (~2%). Upon the addition of saturating X4-gp120 concentrations, we observed a significant reduction in the percentage of monomers and dimers (~82%) and a corresponding increase in nanoclusters composed of ≥3 receptors/particle (~18%) (Figure 1C). This observation aligns with previous findings for CXCL12 (27) As a control, stimulation with CXCL12 resulted in a larger percentage of these nanoclusters (~26%) (Figure 1C). These data correlated with the higher MSI values observed after cell activation (basal 933 a.u.; CXCL12 2,105 a.u., X4-gp120 1,738 a.u.) (Figure 1D). Collectively, these results indicate that X4-gp120 triggers CXCR4 nanoclustering, although to a lesser extent than CXCL12.

## gp120-expressing virus-like particles mediate CXCR4 clustering

Recombinant X4-gp120 alone does not fully replicate the function of HIV-1 Env. Previous studies have shown that the Env consists of gp120 trimers that redistribute and cluster on the surface of virions following proteolytic Gag cleavage during maturation (52). Considering the low number of Env trimers on natural HIV virions (53–55), this clustering is crucial for establishing multiple receptor interactions necessary for virus entry. To mimic the behavior of the virus, we prepared VLPs containing the X4 HIV-1 Env. HEK-293T cells were transiently transfected with pHXB2env, psPAX2, and, when required, a pLentiGFP plasmid that encodes a GFP reporter gene flanked by LTR regions. In this latter case, we generated LVPs because these budding particles contained genetic material and could transduce target cells. Supernatants were collected 48-hours post transfection, and VLPs were purified by ultracentrifugation and resuspended in PBS. The structural integrity of the VLPs was confirmed using negative-stain electron microscopy (Supplementary Figure 6A). Western blot analysis of the samples, culture media, and clarified supernatants confirmed the presence of both gp120 and p24 in VLPs and LVPs (Supplementary Figure 6B). The gp120-containing viral particles bound soluble CD4 (Supplementary Figure 6C) and the corresponding LVPs successfully infected HEK-293CD4 cells, as demonstrated in transduction assays (Supplementary Figure 6D, E). LVPs containing VSVG were utilized as a positive control in these functional assays (Supplementary Figure 6D, E).

Immature HIV-1 particles exhibit reduced entry efficiency (56, 57). This effect may stem from the rigidity of the immature Gag lattice beneath the viral membrane, which hinders membrane fusion (58) interactions between Gag and Env glycoproteins, limiting the lateral mobility of the sparsely distributed Env trimers and, consequently, impairing the clustering necessary for efficient infection (13). Therefore, we evaluated the maturation status of the generated VLPs using STED microscopy. We compared the condensation of Gag and the distribution of Env molecules on the surface of the VLPs with those observed on genetically immature particles and integrase-defective NL4-3ΔIN virions, serving as controls (13). Env proteins were stained with the human mAb 2G12, which specifically recognizes the gp120 domain. To avoid antibody-induced clustering, we used purified Fab fragments of 2G12. The location of individual HIV-1 particles was determined using the human mAb 37G12, which targets the Gag protein and served as a “counterstain” reference

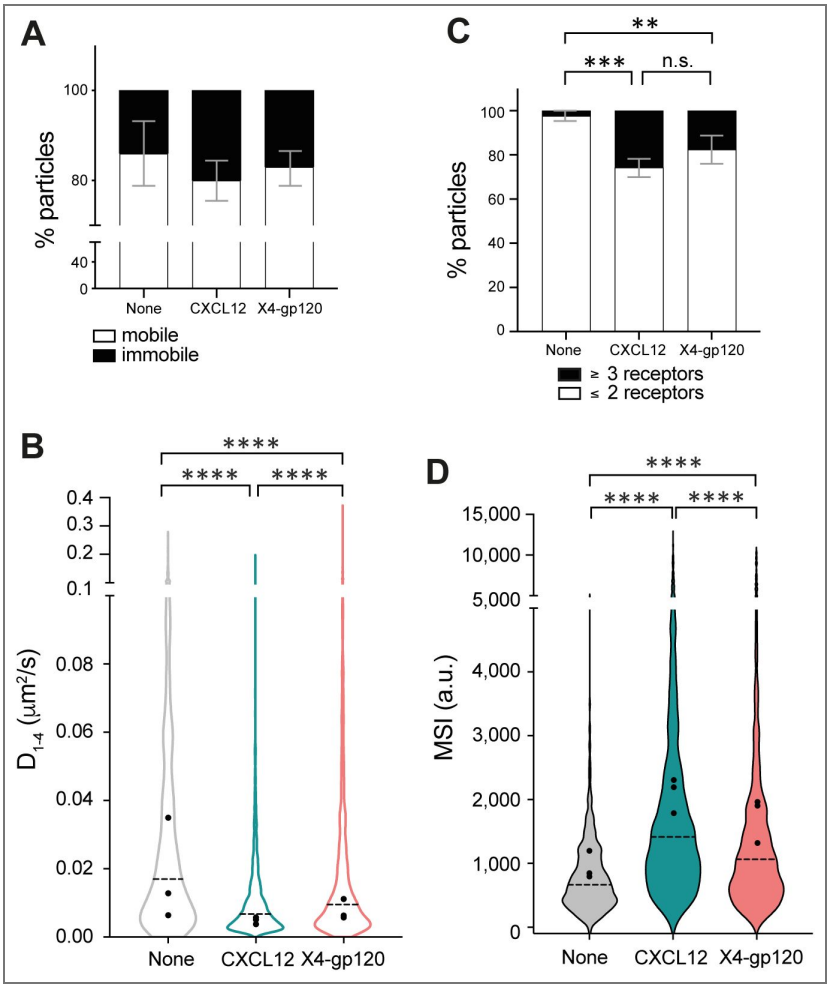


**Figure 1. X4-gp120 modulates CXCR4 dynamics and nanoclustering.**

Single-particle tracking analysis of JKCD4$^{+}$X4$^{-}$ cells transiently transfected with CXCR4-AcGFP on fibronectin (FN)-, FN + CXCL12-, or FN + X4-gp120-coated coverslips (828 particles in 96 cells on FN; 2,997 in 95 cells on FN + CXCL12 and 1,547 in 91 cells on FN + X4- gp120) n = 3. **A)** Percentage of mobile and immobile CXCR4-AcGFP particles at the membrane of cells treated as indicated. **B)** Diffusion coefficients ($D_{1-4}$) of mobile particles at the membrane of cells treated as indicated with the median value of each experiment (black circles) and the median of all trajectories (dotted black lines). (****p ≤ 0.0001). **C)** Frequency of CXCR4-AcGFP particles containing monomers and dimers (≤2) or nanoclusters (≥3), mean ± SD calculated from mean spot intensity (MSI) values of each particle as compared with the value of monomeric CD86-AcGFP (980 ± 86 a.u., **p ≤ 0.01, ***p ≤ 0.001). **D)** Intensity distribution of individual CXCR4-AcGFP trajectories on unstimulated and CXCL12 or X4-gp120-stimulated cells. Graph shows the distribution of all trajectories, with the mean value of each experiment (black circles) and the median of all trajectories (dotted black lines) (n = 3; ****p ≤ 0.0001). Statistical significance was determined by two-way ANOVA in panels A and C and by non- parametric Kruskal-Wallis tests followed by Dunn's test for panels B and D.

(Figure 2A). By assessing Gag condensation, we estimated that ~75% of the VLPs, both gp120-VLPs and Env(-) VLPs, were mature. These percentages were lower for NL4-3ΔIN virions (~50%) and for immature VLPs (~16%) used as controls (Figure 2B). Furthermore, we observed that 26.5% of the gp120-VLPs, 40.2% of the NL4-3ΔIN virions, and 40.5% of the immature VLPs expressed gp120. As a control, the anti-gp120 2G12 Fab did not stain particles lacking the Env (Env(-) VLPs) (Figure 2A, C), confirming the specificity of the staining. Moreover, STED analysis revealed differences in Env distribution between gp120-VLPs and NL4-3ΔIN virions, as previously observed between mature and immature particles (13). Specifically, gp120 staining intensity was higher for NL4-3ΔIN particles than for gp120-VLPs (NL4-3ΔIN 1,786 a.u. vs. gp120-VLPs 1,223 a.u.) (Figure 2D), suggesting a lower expression of Env proteins in the latter or a lower incorporation of the Env proteins into the VLPs. Analysis of gp120 intensity per particle demonstrated that g120-VLPs had lower levels of gp120/particle than NL4-3ΔIN virions (Figure 2E). These data confirmed the mature state of the gp120-VLPs generated and indicated that they contained a reduced number of gp120/particle, similar to or even lower than that found in primary HIV-1 viruses (55).

Next, we employed SPT-TIRF to investigate how gp120-VLPs affect CXCR4 dynamics in JKCD4$^{+}$X4$^{-}$ cells that were transiently transfected with CXCR4-AcGFP (Supplementary video 4-6). Analysis indicated that the gp120-VLPs significantly reduced overall receptor diffusivity (basal, $D_{1-4}$ = 0.025 μm$^2$ s$^{-1}$; Env(-) VLPs, $D_{1-4}$ = 0.017 μm$^2$ s$^{-1}$; gp120-VLPs $D_{1-4}$ = 0.012 μm$^2$ s$^{-1}$) (Figure 3A). In all the cases, most of the trajectories corresponded to confined movement (Supplementary Figure 5B) Under these conditions, we found predominantly CXCR4 monomers and dimers at steady-state, and their proportion decreased upon VLP treatment (basal ~99%; Env(-) VLPs ~91%; gp120-VLPs ~71%). Consequently, the percentage of nanoclusters containing ≥3 receptors/particle increased (~1%, basal; ~9%, VLPs; ~29%, gp120-VLPs) (Figure 3B). These findings were consistent with the MSI values (basal 761 a.u.; Env(-) VLPs 1,150 a.u.; gp120-VLPs 1,898 a.u.) (Figure 3C). Further investigations are needed to elucidate the precise mechanism involved in the effect induced by the Env(-) VLPs on the dynamics of the receptors.

Our results indicated that, similar to the effect triggered by soluble X4-gp120, VLPs containing HIV-1 Env also triggered CXCR4 nanoclustering. To understand the role of CXCR4 clustering in HIV-1 infection, we next analyzed the behavior of the WHIM mutant CXCR4, CXCR4$^{R334X}$, which does not oligomerize in the presence of CXCL12 (28). CXCR4$^{R334X}$ is a natural mutant of CXCR4 that binds CXCL12 (59–61), but is not internalized in response to the ligand; in fact, it is a gain-of-function receptor for this ligand (62). SPT-TIRF-M analysis of JKCD4$^{+}$X4$^{-}$ cells transiently transfected with CXCR4$^{R334X}$-AcGFP (Supplementary video 7-9) demonstrated that, unlike the effect described for CXCL12, the VLPs containing gp120 triggered CXCR4$^{R334X}$ oligomerization (basal MSI 669 a.u.; Env(-) VLPs MSI 909 a.u.; gp120-VLPs MSI 1,730 a.u.) (Figure 4A) and promoted a significant reduction in overall receptor diffusivity (basal, median $D_{1-4}$ = 0.021 μm$^2$s$^{-1}$; gp120-VLPs, median $D_{1-4}$ = 0.014 μm$^2$s$^{-1}$) (Figure 4B) without significant differences in the percentage of trajectories with distinct type of diffusion, again most of them exhibited confined movement (Supplementary Figure 5C). Furthermore, gp120-VLP binding reduced the percentage of CXCR4$^{R334X}$ monomers and dimers (steady-state ~99%; gp120-VLPs ~80%), while concurrently increasing the percentage of nanoclusters containing ≥3 receptors/particle (basal ~1%; gp120-VLPs ~20%) (Figure 4C).

All these data and other previously reported findings (28), indicate that CXCL12 triggers CXCR4 clustering at the cell membrane but does not induce CXCR4$^{R334X}$ oligomers. By contrast, gp120-VLPs binding stabilized CD4 complexes with both CXCR4 and CXCR4$^{R334X}$ and promoted oligomerization of both co-receptors. It is thus plausible that the conformation of CXCR4 and CXCR4$^{R334X}$ may differ between both experimental conditions.

## CD4 expression alters the conformation adopted by CXCR4

Our results support a model where CXCL12 binds to either CXCR4 or CXCR4$^{R334X}$ (28). By contrast, X4-gp120, whether alone or within the viral context, associates these co-receptors when they are complexed with CD4. It is known that CD4/CXCR4 complexes might facilitate co-operative interactions with HIV-1 during viral adsorption and/or entry into human leukocytes (63).

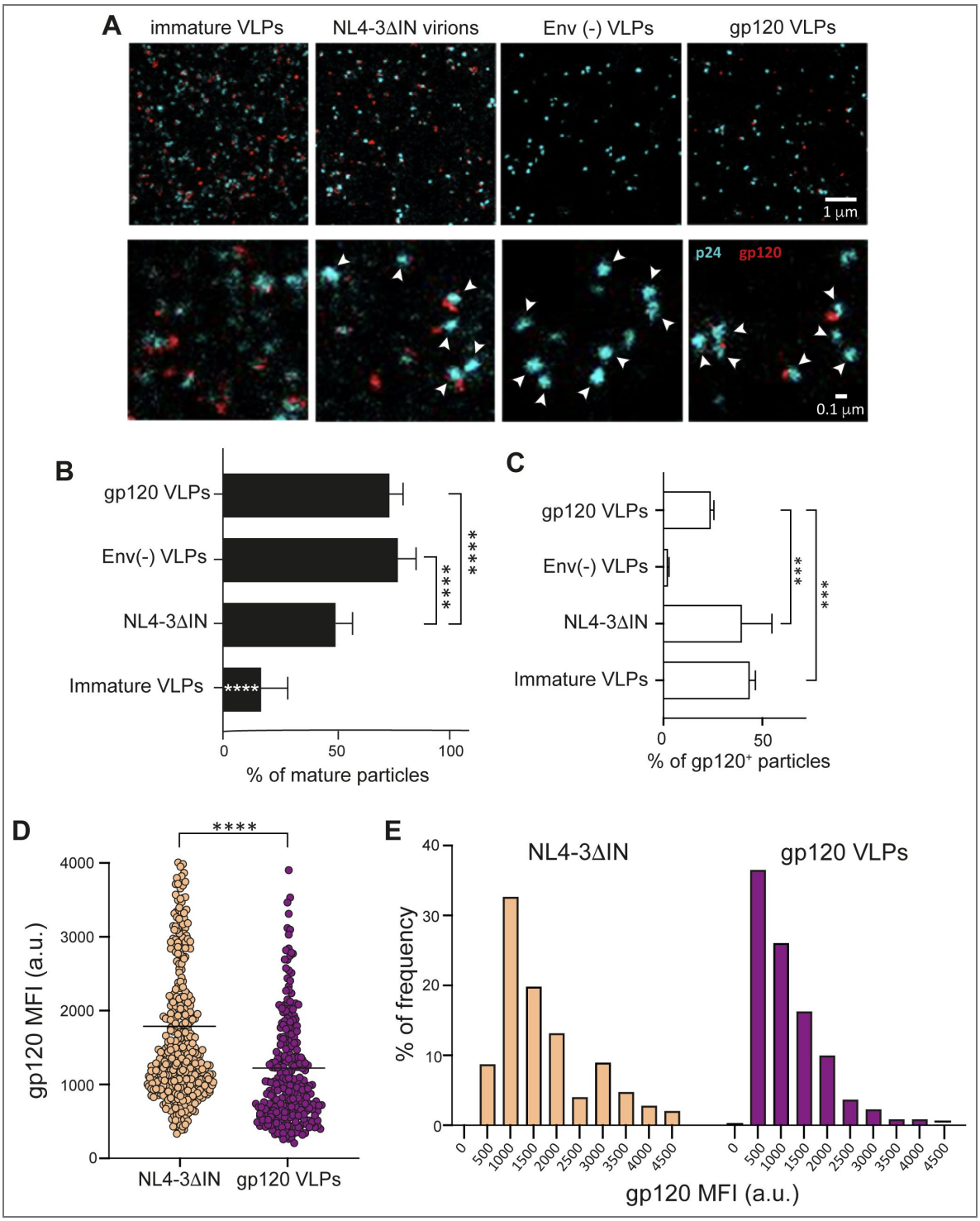


**Figure 2. gp120-VLPs are mature particles that express a low number of Env trimers.**

**A)** Representative images of clarified VLPs visualized by STED microscopy. Upper panels show images of the indicated VLPs stained for Gag p24 (blue) and gp120 (red). Lower panels show 10× magnification of equivalent images. White arrows indicate mature VLPs (p24 condensation). (**B)** Percentage of mature VLPs, analyzed from the images in A) using TrackAnalyzer in ImageJ, based on p24 intensity and aggregation level (mean ± SD; n = 2; ****p ≤ 0.0001; the significance indicated on immature VLPs bar shows the difference with all other conditions). **C)** Percentage of VLPs expressing gp120 on their surface, as analyzed in ImageJ (mean ± SD; n = 2; ***p ≤ 0.001). **D)** Distribution of gp120 mean fluorescence intensity. Each spot corresponds to the mean fluorescence intensity for each analyzed VLP in a.u. The black line represents the mean of all values (****p ≤ 0.0001). **E)** Frequency of gp120 intensity/particle. Statistical significance was determined by one-way-ANOVA followed by Tukey's multiple comparisons test in panels B and C and by Mann-Whitney analysis for panel D.

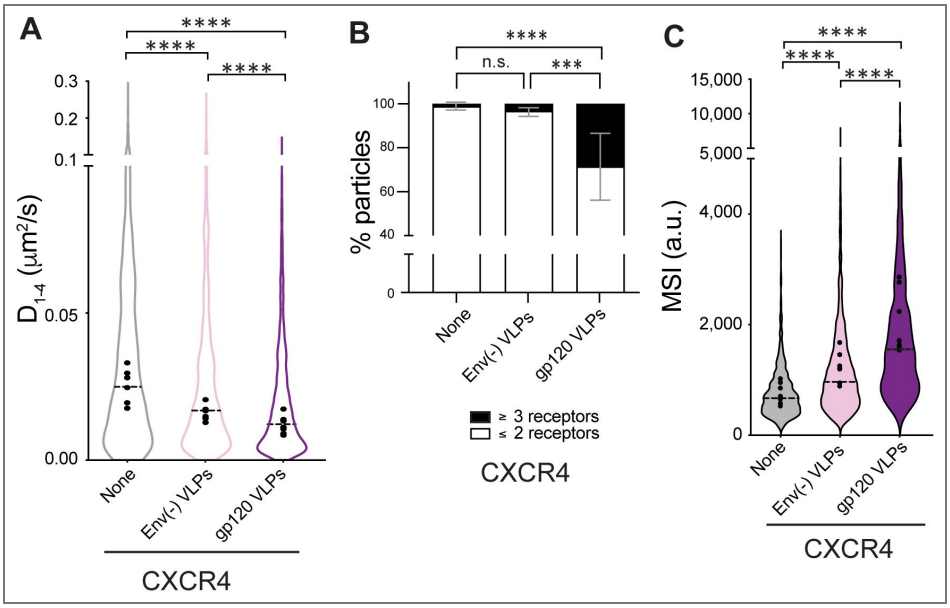


**Figure 3. gp120 VLPs modulate CXCR4 dynamics and nanoclustering.**

Single- particle tracking analysis of JKCD4$^{+}$X4$^{-}$ cells transiently transfected with CXCR4- AcGFP, on fibronectin (FN)-, FN + VLPs-, or FN + gp120 VLPs-coated coverslips (1,087 particles in 159 cells on FN; 1,400 in 153 cells on FN +VLPs and 1,061 in 160 cells on FN + gp120 VLPs) n = 6. **A)** Diffusion coefficients ($D_{1-4}$) of mobile particles at the membrane of cells treated as indicated. Figure shows the mean value of each experiment (black circles) and the median of all trajectories (dotted black lines) (n = 6; ****p ≤ 0.0001). **B)** Frequency of CXCR4-AcGFP particles containing monomers and dimers (≤2) or nanoclusters (≥3) in cells treated as indicated. Mean ± SD calculated from mean spot intensity (MSI) values of each particle as compared with the value of monomeric CD86-AcGFP (980 ± 86 a.u., **p ≤ 0.05, **p ≤ 0.01, ****p ≤ 0.0001). **C)** Intensity distribution (arbitrary units, a.u.) from individual CXCR4-AcGFP trajectories on cells treated as indicated. Graph shows the distribution of all trajectories, with the mean value of each experiment (black circles) and the median of all trajectories (dotted black lines) (n = 6; ****p ≤ 0.0001). Statistical significance was determined by non-parametric Kruskal-Wallis tests followed by Dunn's test for panels A and C, and by two-way ANOVA in panel B.

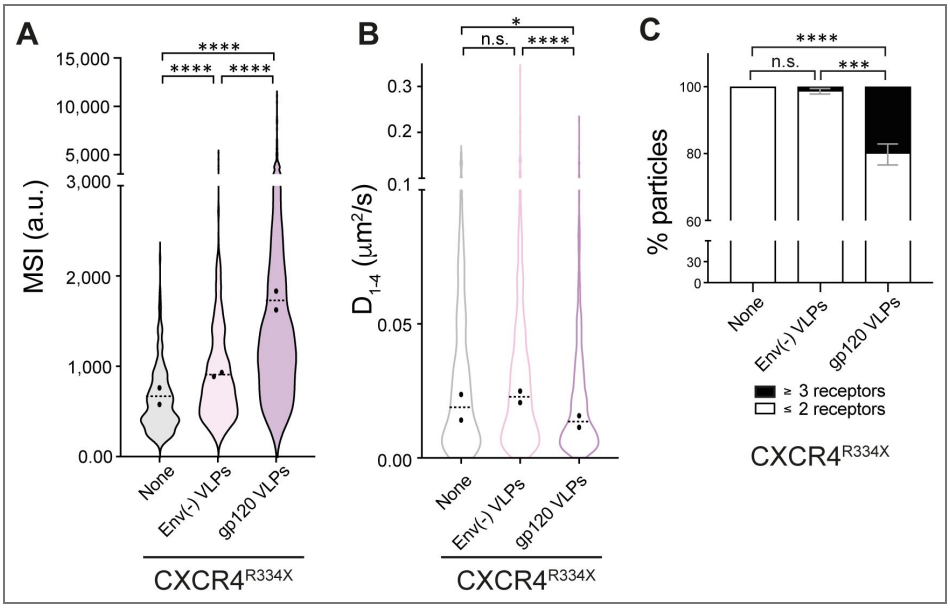


**Figure 4. gp120 VLPs modulate CXCR4$^{R334X}$ dynamics and nanoclustering.**

Single- particle tracking analysis of JKCD4$^{+}$X4$^{-}$ cells transiently transfected with CXCR4$^{R334X}$- AcGFP, on fibronectin (FN)-, FN + VLPs-, or FN + gp120 VLPs-coated coverslips (341 particles in 63 cells on FN; 610 in 54 cells on FN + VLPs and 707 in 63 cells on FN + gp120 VLPs) n = 2. **A)** Intensity distribution (arbitrary units, a.u.) from individual CXCR4$^{R334X}$-AcGFP trajectories on cells treated as indicated. Graph shows the distribution of all trajectories, with the mean value of each experiment (black circles) and the median of all trajectories ± SD (dotted black lines) (n = 2; ****p ≤ 0.0001). **B)** Diffusion coefficients ($D_{1-4}$) of mobile single particle trajectories at the membrane of cells treated as indicated. Figure shows the mean value of each experiment (black circles) and the median of all trajectories (dotted black lines) (n = 2; n.s. not significant, *p ≤ 0.05, ****p ≤ 0.0001). **C)** Frequency of CXCR4$^{R334X}$-AcGFP particles containing monomers plus dimers (≤2) or nanoclusters (≥3), ± SD calculated from mean spot intensity values of each particle as compared with the value of monomeric CD86-AcGFP (*p ≤ 0.05, ***p ≤ 0.001). Statistical significance was determined by non-parametric Kruskal-Wallis tests followed by Dunn's test for panels A and C, and by two-way ANOVA in panel B.

To confirm the interaction between CD4 and CXCR4 (22) and to assess whether CXCR4$^{R334X}$ could also interact with CD4, we conducted FRET analyses. Our results demonstrated positive FRET signals for both complexes: CD4/CXCR4 ($FRET_{50}$=2.71) and CD4/CXCR4$^{R334X}$ ($FRET_{50}$=0.40) (Figure 5A, B). As a control, we observed minimal residual energy transfer in cells co-transfected with CD4-CFP and $5HT_{2B}$-YFP (Figure 5C). The presence of CD4/CXCR4 and CD4/CXCR4$^{R334X}$ heterodimers was also investigated *in silico* using alphaFold3 (64) (Supplementary Figure 7). We focused on the interaction between the transmembrane and intracellular fragments of CD4 and both CXCR4 and CXCR4$^{R334X}$. The predicted template modeling (pTM) scores for both complexes were close to 0.7, suggesting a reliable prediction of these interactions. The modeling also indicated a preferred association of CD4 with CXCR4 between transmembrane helices IV and V, although further analysis is needed to precisely determine the interaction site. These data align with previous reports demonstrating a constitutive association between CD4 and CXCR4 that can influence HIV-1 infection (22, 65–68) and our results extend this observation to the naturally occurring CXCR4$^{R334X}$ mutant. Furthermore, we observed increased FRET efficiency in both CD4-CXCR4 and CD4-CXCR4$^{R334X}$ complexes upon gp120-VLPs binding (Figure 5D, E), confirming that the VLPs induce conformational changes in these heterodimers.

Productive HIV-1 infection of $CD4^+$ cells markedly diminishes cell-surface expression of CD4 (69, 70). However, the impact on chemokine receptors is less clear. While some studies report a complete loss of CCR5 surface staining on cells chronically infected with R5 viruses (71) the effect on CXCR4 varies (71, 72). Using flow cytometry, we investigated how stimulation with X4-gp120 affects the cell-surface expression of CD4, CXCR4, and CXCR4$^{R334X}$. Consistent with previous findings (73), CXCL12 induced rapid internalization of CXCR4 without altering CXCR4$^{R334X}$ levels at the cell surface. By contrast, X4-gp120 caused a gradual, slight decrease in the surface expression of both receptors. Furthermore, CXCL12 did not affect CD4 surface levels, whereas X4-gp120 induced a gradual decline in CD4 expression (Figure 6A, B).

Taken together, our FRET and internalization experiments suggest that the effects of X4-gp120 on CXCR4 and CXCR4$^{R334X}$ differ from those triggered by CXCL12 and are dependent on their interaction with CD4.

Next, we investigated whether CD4/CXCR4$^{R334X}$ complexes could also support primary HIV-1 infection. Flow cytometry analysis showed no significant difference in the ability of Jurkat cells expressing either CXCR4 or CXCR4$^{R334X}$ to bind X4-gp120 (Figure 7A). In agreement, *in vitro* fusion assays using cells expressing CD4/CXCR4 or CD4/CXCR4$^{R334X}$, and target cells expressing HIV pHXB2 Env, demonstrated a significant increase in fusion events and syncytium formation in both Jurkat cell types (Figure 7B, C). We then tested whether PBMCs isolated from a WHIM patient and healthy donors were equally susceptible to infection by a primary X4 HIV-$1_{NL4-3}$ viral strain. We first analyzed the expression of CD4, and CXCR4 or CXCR4$^{R334X}$ on these PBMC samples by flow cytometry (Supplementary Figure 8A-C). Subsequently, cells were stimulated with PHA and IL-2, and 48 hours later, inoculated with a primary X4 HIV-$1_{NL4-3}$ virus at a MOI of 0.001 for 120 minutes. ELISA measurements of p24 levels in the culture medium at various time points revealed similar viral infection rates in both Healthy and WHIM PBMCs (Figure 7D).

Collectively, these data indicate that T cells from a WHIM patient exhibit similar infection and viral replication rates with those isolated from healthy donors. Furthermore, these data suggest that HIV-1 might modulate the conformation adopted by CXCR4 at the cell membrane, which is associated with HIV-1 infection. The CXCR4 conformation stabilized by HIV-1 binding likely differs from that induced by CXCL12 binding and therefore supports a direct effect of the interactions with CD4 in establishing a permissive conformation of CXCR4 for HIV-1 infection.

# Discussion

The process of HIV-1 infection begins with the binding of the trimeric HIV-1 Env glycoprotein to the CD4 receptor on the target cell surface (74–76). Research indicates that when the viral and cellular membranes are spatially distant, the HIV-1 Env trimers initially engage only a single CD4 molecule, and as the Env moves closer to the membrane and adopts an open conformation it gains

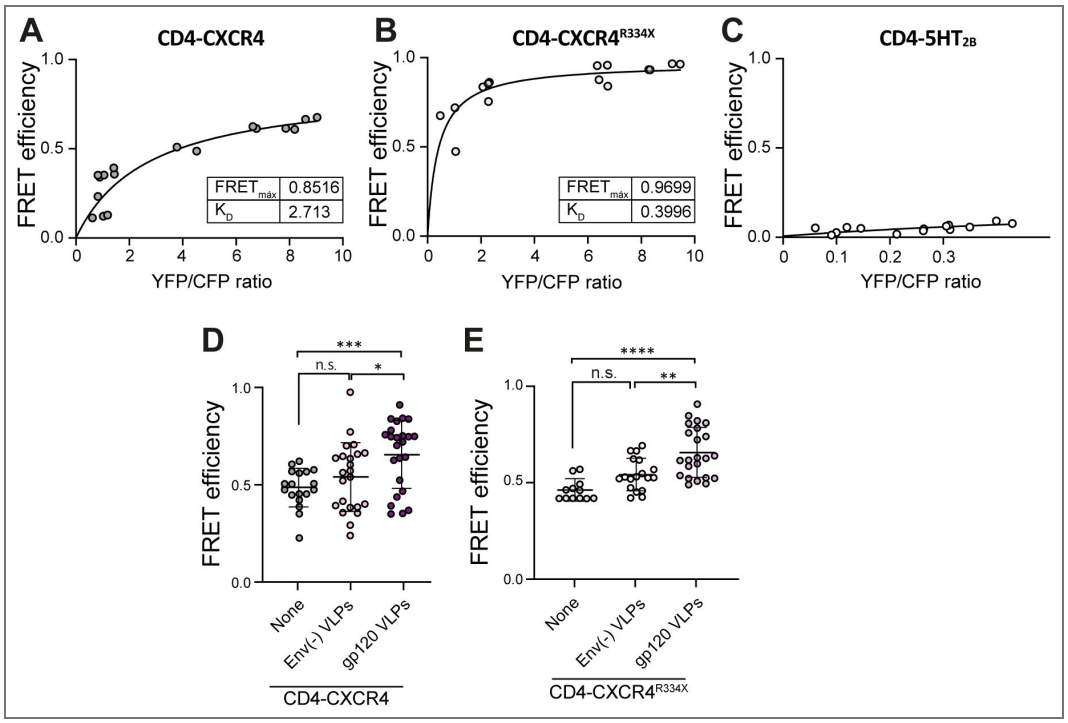


**Figure 5. CD4 forms heterodimers with CXCR4 and CXCR4$^{R334X}$.**

FRET saturation curves generated using HEK-293T cells transiently transfected with a constant amount of CD4-CFP DNA (2 µg) and increasing amounts of **A)** CXCR4-YFP (0.5–8.0 µg), **B)** CXCR4$^{R334X}$-YFP (0.5–8.0 µg) or **C)** 5HT$_{2B}$ DNA (0.5–12 µg). $K_D$ and $FRET_{max}$ values were calculated using a nonlinear regression equation for a single binding-site model (n = 2). **D)** FRET efficiency in HEK-293 cells transiently transfected with CXCR4-YFP/ CD4-CFP (ratio 15:9), in the absence or presence of gp120 VLPs or Env(-) VLPs. Data shows FRET efficiency (arbitrary units, a.u.) (mean ± SD; n = 3; n.s. not significant, *p ≤ 0.05, ***p ≤ 0.001). **E)** FRET efficiency in HEK-293 cells transiently transfected with CXCR4$^{R334X}$-YFP/CD4-CFP (ratio 15:9), in the absence or presence of gp120-VLPs or Env(-) VLPs. Data shows FRET efficiency (a.u.) (mean ± SD; n = 3; n.s. not significant, *p ≤ 0.05, ***p ≤ 0.001, ****p ≤ 0.0001). Statistical significance was determined by unpaired t-test in panels D and E.

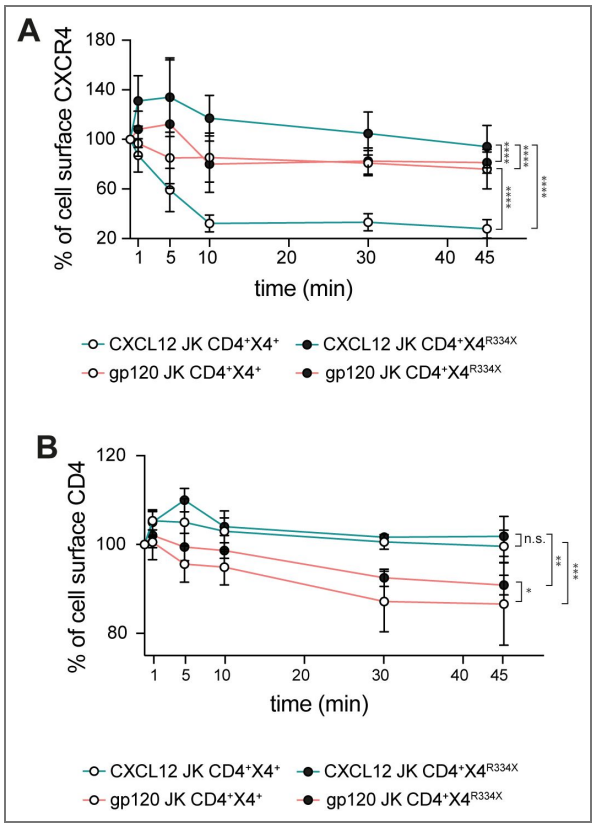


**Figure 6. X4-gp120 promote similar internalization patterns of CXCR4 and CXCR4$^{R334X}$ receptors.**

**A)** Surface receptor expression of CXCR4 (white dots) or CXCR4$^{R334X}$ (black dots), after stimulation with CXCL12 (blue lines) or X4-gp120 (red lines). Results show mean ± SD of the percentage of receptor expression at the cell surface (n = 3). **B)** Surface receptor expression of CD4 in JK CD4$^+$ CXCR4$^+$ (white dots) or JK CD4$^+$ CXCR4$^{R334X}$ (black dots), after stimulation with CXCL12 (blue lines) or X4-gp120 (red lines). Results show mean ± SD of the percentage of receptor expression at the cell surface (n = 3). Statistical significance was determined by one-way-ANOVA of AUC (*p ≤ 0.05, **p ≤ 0.01).

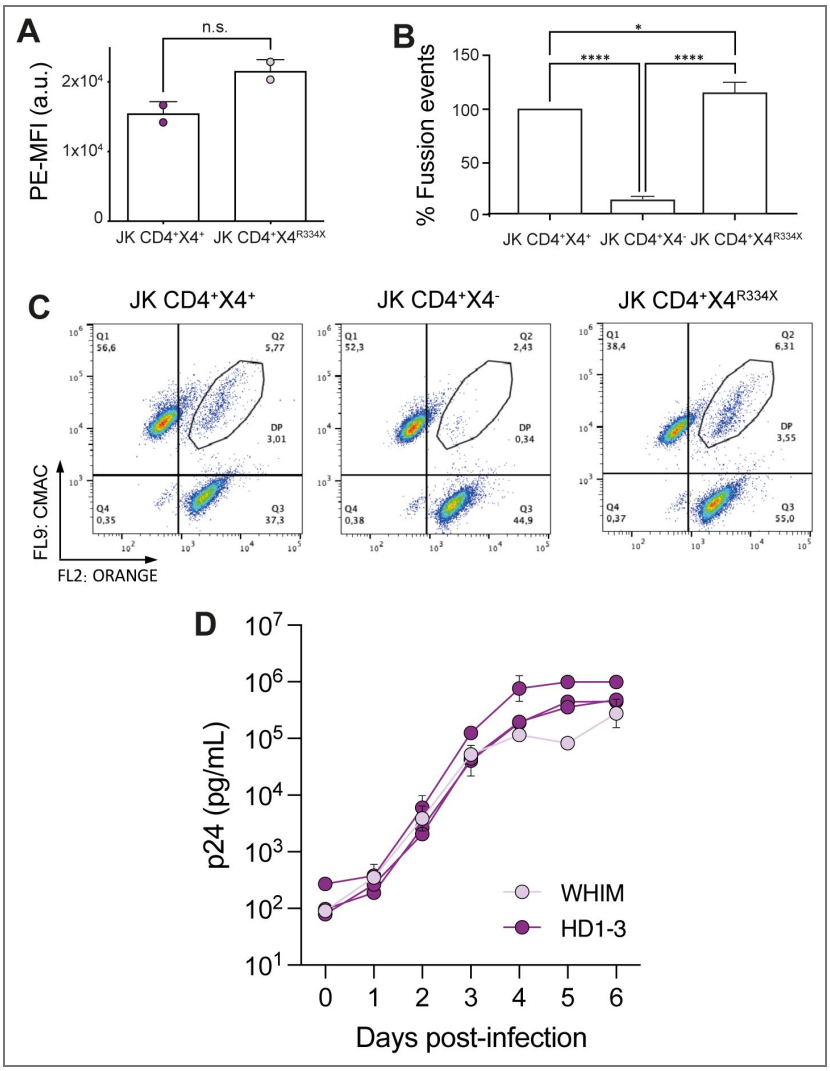


**Figure 7. CD4/CXCR4 and CD4/CXCR4$^{R334X}$ complexes support similar HIV-1 infection.**

The presence of CXCR4$^{R334X}$ on JKCD4$^{+}$ cells does not alter gp120 binding and increases fusion events with target cells expressing HIV pHXB2 envelope. **A)** Binding of X4-gp120 to target cells expressing CD4 and CXCR4 or CD4 and CXCR4$^{R334X}$ analyzed by flow cytometry. Cells were incubated with 0.3 µg/mL of X4- gp120 at 37°C for 30 minutes. Data show MFI (arbitrary units, a.u.) mean ± SD; (n = 2). Statistical significance was determined using Student's t-test (n.s.= not significant). **B)** Cell-cell fusion between JKHXBc2-expressing HIV-1 envelope and different target cells (JKCD4$^{+}$CXCR4$^{+}$, JKCD4$^{+}$CXCR4$^{-}$ and JKCD4$^{+}$CXCR4$^{R334X}$). Prior to co-culture, each cell type was loaded with the corresponding cell-tracker. Data show the percentage of fusion events ± SD (n = 6). We used as reference the fusions events detected in JKCD4$^{+}$CXCR4$^{+}$ cells (100%). Statistical significance was determined by one-way- ANOVA (*p < 0.05, ****p ≤ 0.0001). **C**) Representative biparametric histograms from cells in B showing CMAC *versus* orange fluorophores. **D**) Human PBMCs isolated from a WHIM patient (WHIM) and three healthy donors (HD1-3) in two independent experiments were infected with X4-pseudotyped HIV-1$_{NL4-3}$ (MOI: 0.001). At 2 hours post infection (p.i.), supernatant samples were obtained at different time points (days post-infection) and p24 levels (pg/mL) in each sample were determined using a commercial ELISA. Results show mean ± SD (n = 2).

the ability to bind a second and a third CD4 molecule (24). CD4 binding thus induces critical conformational changes within the gp120 subunit of Env that enable subsequent engagement of the co-receptors CCR5 or CXCR4. Receptor and co-receptor engagement trigger further conformational changes in the Env gp41 subunits, ultimately mediating the necessary fusion of the viral and host cell membranes.

Competitive receptor inhibitors, such as soluble synthetic CD4 (sCD4), synthetic CD4 peptides, and anti-CD4 binding site antibodies have been shown to effectively block infection both *in vitro* (77, 78) and *in vivo* (79, 80). Notably, virus-like nanoparticles displaying clustered membrane-associated CD4 demonstrated significantly greater efficacy at blocking infection compared with sCD4, CD4-Ig, or the broadly neutralizing monoclonal antibody 3BNC117 (81). These findings collectively suggest that the virus may induce CD4 clustering to promote cell infection. Consistent with this idea, single-molecule super-resolution imaging has revealed that CD4 molecules on the cell membrane exist predominantly as individual molecules or small clusters (up to 4 molecules), and that the size and number of these clusters increase upon virus binding or gp120 activation (19). These data therefore support a model where viral binding triggers a nanoscale reorganization of CD4 on the plasma membrane, a process necessary for cell infection. This observation aligns with substantial evidence indicating that various cell-surface receptors are organized into clusters (23, 82). For instance, T-cell receptors on T cells coalesce into nanoclusters within and around immune synapses prior to signal transduction (83, 84). Receptor clustering has been also demonstrated for numerous other transmembrane receptors, such as neurotransmitter receptors (85) and immune receptors (86, 87). Furthermore, studies analyzing receptor dynamics during cell movement using SPT have shown that chemokine-mediated receptor clustering is essential for cells to accurately sense chemoattractant gradients (27, 28).

Here, using SPT-TIRF-M analysis on Jurkat cells, we found that both recombinant X4-gp120 and VLPs displaying X4 HIV-1 Env (with fewer gp120 molecules) actively promote CXCR4 clustering and modify its membrane dynamics in a CD4-dependent manner. Our data show that, similar to the effect of CXCL12, gp120 binding to CXCR4 leads to a significant decrease in the number of monomers and dimers, while increasing the proportion of larger, generally immobile nanoclusters. Previous studies utilizing immunoelectron microscopy have suggested that CCR5, CXCR4, and CD4 are mainly localized on microvilli and tend to form distinct, uniform microclusters in all cell types examined (63). This clustering is thought to enhance co-operative interactions with HIV-1 during virus adsorption and subsequent entry into human leukocytes (63). Single-molecule force spectroscopy has also revealed that the force and duration required to break apart the gp120/CCR5/CD4 complex are greater than those required for the gp120/CD4 bond (88). The formation of CCR5/CD4/CXCR4 oligomers is implicated in reducing the infectivity of X4 HIV-1 in cells that also express CCR5 (22).

The data suggest that exposure to HIV-1 triggers several rearrangements of cell receptors, highlighting the significance of these changes in facilitating viral entry into target cells. Receptor clustering, a process known to enhance cell sensitivity (89), also promotes efficient cell signal transmission (90), and increases the robustness of signaling systems (91). Indeed, it is well established that HIV-1 promotes CD4- and CXCR4- mediated signaling events that facilitate viral entry and infection of host cells (39, 92–95). We observed that gp120 triggered the phosphorylation of Lck, Akt, and ERK1/2, and promoted cell polarization, although this latter effect was less pronounced than that induced by CXCL12. Furthermore, in lipid bilayer assays using ICAM-1 as a substrate, gp120 mediated Jurkat cell adhesion but did not significantly promote cell migration compared with CXCL12. While soluble gp120 has been used to investigate certain HIV- 1 effects on cells (39, 43, 96), employing saturating concentrations of the glycoprotein might lead to non-specific effects on the dynamics of receptors and co-receptors at the cell membrane. Moreover, the conformation of recombinant gp120 may not accurately reflect its physiological structure on intact HIV-1 particles. Within virions, the Env glycoprotein forms heterotrimeric gp120 non-covalently associated with three gp41 molecules. To address these limitations, we generated VLPs displaying the X4 HIV-1 Env. Super-resolution microscopy confirmed the maturity of the gp120-VLPs, expressing a very low number of gp120 trimers on their surface, even fewer than the 7 to 14 Env

trimers per virus particle previously reported on primary isolated virions (54, 97, 98) Similar to soluble recombinant gp120, these VLPs also induced CXCR4 clustering and altered receptor dynamics. These findings thus confirm that the effects observed with X4- gp120 are not artifacts resulting from the conformation of the soluble gp120 or to the use of saturating concentrations. Receptor clustering was initiated through binding of gp120- VLPs to CD4 and CXCR4, as neither X4-gp120 nor the VLPs associated with CXCR4 in the absence of CD4. We confirmed this using a mutant CXCR4, $CXCR4^{R334X}$, which does not oligomerize in the presence of CXCL12 (28). $CXCR4^{R334X}$ is found in cells of patients with WHIM syndrome, a rare combined immunodeficiency characterized by the presence of warts, hypogammaglobulinemia, recurrent bacterial infections and myelokathexis symptoms (29). In these patients, the inability of CXCL12 to induce receptor oligomerization leads to defects in actin dynamics, preventing proper sensing of chemoattractant gradients (28, 99). We investigated how VLPs containing the X4 HIV-1 Env affected the dynamics of $CXCR4^{R334X}$ in cells expressing CD4. Surprisingly, the X4 HIV-1 Env caused a significant reduction in $CXCR4^{R334X}$ monomers and dimers, while increasing the proportion of larger nanoclusters, which were generally immobile. These findings suggest that CXCL12 and gp120 VLPs have different effects on chemokine receptor dynamics, leading us to hypothesize that the structure of CXCR4, whether or not it is associated with CD4, could explain these observations. AlphaFold predictions and FRET analysis confirmed the formation of CD4/CXCR4 complexes (22) and supported the existence of $CD4/CXCR4^{R334X}$ heterodimers. In both cases, gp120-VLPs binding altered the conformations. These findings correlate with the syncytia formation observed in *in vitro* fusion experiments between cells expressing the X4 HIV-1 Env and target cells expressing either CD4/CXCR4 or $CD4/CXCR4^{R334X}$, and with the infection of PBMCs from both WHIM patients and healthy donors when incubated with primary X4-HIV-1. These findings also indicate that WHIM mutations do not protect against HIV-1 infection, consistent with a previous *in vitro* study showing that $CD4^{+}$U87 cells expressing $CXCR4^{R334X}$ or CXCR4 are equally susceptible to a luciferase-expressing pseudotyped virus infection (60). To better reflect natural infection kinetics, we employed fully replication-competent viruses rather than pseudotyped systems. Furthermore, we monitored viral dynamics over a seven-day period, providing a longitudinal perspective that extends beyond the limitations of a standard 24-hour snapshot. Beyond inducing CXCR4 aggregation, we observed that X4-gp120 promoted the internalization of CD4 and CXCR4 and, surprisingly, also triggered the internalization of $CXCR4^{R334X}$. This mutant receptor cannot internalize in response to CXCL12 because it lacks the last 19 C- terminal amino acids, which are necessary for GRK-mediated Ser/Thr phosphorylation and β-arrestin recruitment (29, 100). Some studies suggest that HIV-1 glycoproteins can reduce CD4 and CXCR4 levels during HIV-1 entry (72, 101, 102), proposing receptor- mediated endocytosis as an alternative HIV-1 entry mechanism (103–108). Other reports even indicate a ligand-mediated co-endocytosis of CD4 and the chemokine receptors during HIV-1 entry (109–111). HIV-1-mediated endocytosis might also explain the reduction of CD4 and $CXCR4^{R334X}$ at the cell membrane and the similar infection rates in PBMCs from WHIM patients and healthy donors. Although direct evidence for the internalization of CD4 and CXCR4 as complexes is lacking, their co-localization in lipid rafts during HIV-1 infection (32, 112, 113) and their ability to form heterocomplexes (22) strongly suggest they could be endocytosed together. Therefore, we hypothesize that gp120 binding to CD4 stabilizes CD4/CXCR4 complexes, and that the conformation of CXCR4 within these complexes might differ from that of CXCR4 homodimers.

We also detected a residual but significant effect of Env(-) VLPs on the dynamics of both CXCR4 and of $CXCR4^{R334X}$. This is likely not receptor-mediated, as these control VLPs lacked the X4 HIV-1 Env. While further experiments are needed, a potential interaction between the lipids and or cell adhesion molecules derived from the cells where the virions were produced, and those in the cell membrane could explain this observation. It is well established that the lipid composition of the cell membrane influences ligand- mediated chemokine receptor oligomerization and dynamics (114, 115). Additionally, glycosaminoglycans, such as heparin and heparan sulphate, might play a role in the attachment of virions to various cell types (116–118). Although their effects on R5

strains are debated (119–121), the concentrations of these glycosaminoglycans vary considerably between cells (122). Besides, some viruses bind lectins at the cell membrane, for instance some microdomains of C-type lectin DC-SIGN have been described as portals for HIV- 1 entry (123, 124).

Our data indicate that HIV-1 not only affects CD4 dynamics, which is well known, but also alters the spatial distribution and dynamics of CXCR4 in a manner distinct from the effects of its natural ligand, CXCL12. While HIV-1 binding involves CD4/CXCR4 complexes, CXCL12 binds exclusively to CXCR4, potentially leading to different effects on CXCR4 conformations. These findings might also explain why HIV-1 induced the endocytosis of both CD4/CXCR4 and CD4/CXCR4$^{R334X}$ complexes, whereas CXCL12 did not mediate the internalization of either CD4 or the CD4/CXCR4$^{R334X}$ complex. This suggests that the interaction of both co-receptors with CD4 may result in different conformations of CXCR4 and CXCR4$^{R334X}$ compared with their respective homodimers. The interaction motif between CD4 and CXCR4 should be considered a crucial target for disrupting complex dynamics at the cell membrane, potentially opening new avenues for anti-HIV-1 therapies.

## Data availability

All data generated or analysed during this study are included in the manuscript, figures, figure supplements and source data files.

## Acknowledgements

This work was supported by grants from the Spanish Ministry of Science and Innovation (PID2020-114980RB-I00 and PID2023-146301OB-I00) to MM and (PID2022- 140651NB-I00) to CS, and (PID2022-139271OB-I00 and CB21/13/00063) to JM-P. EG-C and BS were supported by the program Apoyos Centros de Excelencia S.O. of the Spanish Ministry of Science and Innovation (SEV-2017-0712). AQ-F and SRG ere included in the doctoral program of the Department of Molecular Biosciences and of Biology, respectively, Universidad Autónoma de Madrid, and are supported by the Fondo de Personal Investigador (FPI) program of the Spanish Ministry for Science and Innovation (PRE2018-083201 and PRE2019-087966, respectively). EAB is included in the doctoral program of Biomedicine, University of Barcelona, and is supported by the FPI program of the Spanish Ministry for Science and Innovation (PRE2022-000847). RA- B is supported by the Garantía Juvenil program of the Regional Government of Madrid, Spain (CAM20_CNB_AI_07). LIGG receives funding from Institute of Health, Carlos III co-funded by Fondos FEDER Project FIS PI21/01642. We also acknowledge the technical help of the Advance Light Microscopy Unit at the CNB/CSIC.

## Additional files

***Supplementary video 1***

***Supplementary video 2***

***Supplementary video 3***

***Supplementary video 4***

***Supplementary video 5***

***Supplementary video 6***

***Supplementary video 7***

***Supplementary video 8***

***Supplementary video 9***

***Supplementary figures 1-8***

***Supplementary Video legends***

# Additional information

## Funding


| Funder | Grant reference number | Author |
|---|---|---|
| MEC \| Spanish National Plan for Scientific and Technical Research and Innovation (Plan Estatal de Investigación Científica y Técnica y de Innovación) | PID2020-114980RB-I00 | Mario Mellado |
| Fundación para el Conocimiento Madri+d (Madrimasd Knowledge Foundation) | CAM20_CNB_AI_07 | Rosa Ayala-Bueno |
| Federación Española de Enfermedades Raras (FEDER) | FIS PI21/01642 | Luis Ignacio González-Granado |
| MEC \| Spanish National Plan for Scientific and Technical Research and Innovation (Plan Estatal de Investigación Científica y Técnica y de Innovación) | PID2023-146301OB-I00 | Mario Mellado |
| MEC \| Spanish National Plan for Scientific and Technical Research and Innovation (Plan Estatal de Investigación Científica y Técnica y de Innovación) | PID2022-140651NB-I00 | César Santiago |
| MEC \| Spanish National Plan for Scientific and Technical Research and Innovation (Plan Estatal de Investigación Científica y Técnica y de Innovación) | PID2022-139271OB-I00 | Javier Martinez-Picado |
| Centro de Investigación Biotecnológica en Red de Enfermedades Infecciosas (CIBERINFEC) | CB21/13/00063 | Javier Martinez-Picado |
| CSIC \| Centro Nacional de Biotecnología (CNB) | SEV-2017-0712 | Eva M García-Cuesta |
| MEC \| Spanish National Plan for Scientific and Technical Research and Innovation (Plan Estatal de Investigación Científica y Técnica y de Innovación) | PRE2018-083201 | Sofia Gardeta |
| MEC \| Spanish National Plan for Scientific and Technical Research and Innovation (Plan Estatal de Investigación Científica y Técnica y de Innovación) | PRE2019-087966 | Adriana Quijada-Freire |
| MEC \| Spanish National Plan for Scientific and Technical Research and Innovation (Plan Estatal de Investigación Científica y Técnica y de Innovación) | PRE2022-000847 | Eva Armendariz-Burgoa |


## Author ORCID iDs

**Ricardo Villares**: https://orcid.org/0000-0001-7562-6700
**Javier Martinez-Picado**: https://orcid.org/0000-0002-4916-2129
**Mario Mellado**: https://orcid.org/0000-0001-6325-1630

# References

1. **Kowalski M.,** et al. (1987) Functional regions of the envelope glycoprotein of human immunodeficiency virus type 1. *Science* **237**:1351-1355 https://doi.org/10.1126/science.3629244 | PubMed

2. **Lu M.,** Blacklow S. C., Kim P. S. (1995) A trimeric structural domain of the HIV-1 transmembrane glycoprotein. *Nature Structural Biology* **2**:1075-1082 https://doi.org/10.1038/nsb1295-1075 | PubMed
3. **Choe H.,** et al. (1996) The beta-chemokine receptors CCR3 and CCR5 facilitate infection by primary HIV-1 isolates. *Cell* **85**:1135-1148 https://doi.org/10.1016/s0092-8674(00)81313-6 | PubMed
4. **Feng Y.,** Broder C. C., Kennedy P. E., Berger E. A. (1996) HIV-1 entry cofactor: functional cDNA cloning of a seven-transmembrane, G protein-coupled receptor. *Science* **272**:872-877 https://doi.org/10.1126/science.272.5263.872 | PubMed
5. **Wolinsky S. M.,** et al. (1996) Adaptive evolution of human immunodeficiency virus- type 1 during the natural course of infection. *Science* **272**:537-542 https://doi.org/10.1126/science.272.5261.537 | PubMed
6. **Lu Z. H.,** et al. (1997) Evolution of HIV-1 coreceptor usage through interactions with distinct CCR5 and CXCR4 domains. *Proc Natl Acad Sci U S A* **94**:6426-6431 https://doi.org/10.1073/pnas.94.12.6426 | PubMed
7. **Connor R. I.,** Mohri H., Cao Y., Ho D. D. (1993) Increased viral burden and cytopathicity correlate temporally with CD4+ T-lymphocyte decline and clinical progression in human immunodeficiency virus type 1-infected individuals. *J Virol* **67**:1772-1777 https://doi.org/10.1128/jvi.67.4.1772-1777.1993 | PubMed
8. **Carter C. C.,** et al. (2011) HIV-1 Utilizes the CXCR4 Chemokine Receptor to Infect Multipotent Hematopoietic Stem and Progenitor Cells. *Cell Host Microbe* **9**:223-234 https://doi.org/10.1016/j.chom.2011.02.005 | PubMed
9. **Landau N. R.,** Warton M., Littman D. R. (1988) The envelope glycoprotein of the human immunodeficiency virus binds to the immunoglobulin-like domain of CD4. *Nature* **334**:159-162 https://doi.org/10.1038/334159a0 | PubMed
10. **Arthos J.,** et al. (1989) Identification of the residues in human CD4 critical for the binding of HIV. *Cell* **57**:469-481 https://doi.org/10.1016/0092-8674(89)90922-7 | PubMed
11. **Zhang W.,** et al. (1999) Conformational changes of gp120 in epitopes near the CCR5 binding site are induced by CD4 and a CD4 miniprotein mimetic. *Biochemistry* **38**:9405-9416 https://doi.org/10.1021/bi990654o | PubMed
12. **Doms R. W.,** Moore J. P. (2000) HIV-1 membrane fusion: targets of opportunity. *J Cell Biol* **151** https://doi.org/10.1083/jcb.151.2.f9 | PubMed
13. **Chojnacki J.,** et al. (2012) Maturation-dependent HIV-1 surface protein redistribution revealed by fluorescence nanoscopy. *Science* **338**:524-528 https://doi.org/10.1126/science.1226359 | PubMed
14. **Buzon V.,** et al. (2010) Crystal structure of HIV-1 gp41 including both fusion peptide and membrane proximal external regions. *PLoS Pathog* **6**:1-7 https://doi.org/10.1371/journal.ppat.1000880 | PubMed
15. **Pancera M.,** et al. (2010) Structure of HIV-1 gp120 with gp41-interactive region reveals layered envelope architecture and basis of conformational mobility. *Proc Natl Acad Sci U S A* **107**:1166-1171 https://doi.org/10.1073/pnas.0911004107 | PubMed
16. **Garg H.,** Viard M., Jacobs A., Blumenthal R. (2011) Targeting HIV-1 gp41-induced fusion and pathogenesis for anti-viral therapy. *Curr Top Med Chem* **11**:2947-2958 https://doi.org/10.2174/156802611798808479 | PubMed
17. **Barrero-Villar M.,** et al. (2009) Moesin is required for HIV-1-induced CD4-CXCR4 interaction, F-actin redistribution, membrane fusion and viral infection in lymphocytes. *J Cell Sci* **122**:103-113 https://doi.org/10.1242/jcs.035873 | PubMed
18. **Jiménez-Baranda S.,** et al. (2007) Filamin-A regulates actin-dependent clustering of HIV receptors. *Nat Cell Biol* **9**:838-846 https://doi.org/10.1038/ncb1610 | PubMed
19. **Yuan Y.,** et al. (2021) Single-Molecule Super-Resolution Imaging of T-Cell Plasma Membrane CD4 Redistribution upon HIV-1 Binding. *Viruses* **13** https://doi.org/10.3390/v13010142 | PubMed

20. **Lapham C. K.,** et al. (1996) Evidence for cell-surface association between fusin and the CD4-gp120 complex in human cell lines. *Science* **274**:602-605 https://doi.org/10.1126/science.274.5287.602 | PubMed

21. **Ugolini S.,** et al. (1997) HIV-1 gp120 Induces an Association Between CD4 and the Chemokine Receptor CXCR4'. *The Journal of Immunology* **159**:3000-3008 https://doi.org/10.4049/jimmunol.159.6.3000 | PubMed

22. **Martínez-Muñoz L.,** et al. (2014) CCR5/CD4/CXCR4 oligomerization prevents HIV-1 gp120IIIB binding to the cell surface. *Proc Natl Acad Sci U S A* **111** https://doi.org/10.1073/pnas.1322887111 | PubMed

23. **Hartman N. C.,** Groves J. T. (2011) Signaling clusters in the cell membrane. *Curr Opin Cell Biol* **23**:370-376 https://doi.org/10.1016/j.ceb.2011.05.003 | PubMed

24. **Li W.,** et al. (2023) HIV-1 Env trimers asymmetrically engage CD4 receptors in membranes. *Nature* **623**:1026-1033 https://doi.org/10.1038/s41586-023-06762-6 | PubMed

25. **Krummel M. F.,** Sjaastad M. D., Wulfing C. W., Davis M. M. (2000) Differential clustering of CD4 and CD3zeta during T cell recognition. *Science* **289**:1349-1352 https://doi.org/10.1126/science.289.5483.1349 | PubMed

26. **Kao H.,** Lin J., Littman D. R., Shaw A. S., Allen P. M. (2008) Regulated movement of CD4 in and out of the immunological synapse. *J Immunol* **181**:8248-8257 https://doi.org/10.4049/jimmunol.181.12.8248 | PubMed

27. **Martínez-Muñoz L.,** et al. (2018) Separating Actin-Dependent Chemokine Receptor Nanoclustering from Dimerization Indicates a Role for Clustering in CXCR4 Signaling and Function. *Mol Cell* **70**:106-119.e10 https://doi.org/10.1016/j.molcel.2018.02.034 | PubMed

28. **García-Cuesta E. M.,** et al. (2022) Altered CXCR4 dynamics at the cell membrane impairs directed cell migration in WHIM syndrome patients. *Proc Natl Acad Sci U S A* **119** https://doi.org/10.1073/pnas.2119483119 | PubMed

29. **Liu Q.,** et al. (2012) WHIM syndrome caused by a single amino acid substitution in the carboxy-tail of chemokine receptor CXCR4. *Blood* **120**:181-189 https://doi.org/10.1182/blood-2011-12-395608 | PubMed

30. **García-Cuesta E. M.,** et al. (2022) Altered CXCR4 dynamics at the cell membrane impairs directed cell migration in WHIM syndrome patients. *Proc Natl Acad Sci U S A* **119** https://doi.org/10.1073/pnas.2119483119 | PubMed

31. **Gardeta S. R.,** et al. (2022) Sphingomyelin Depletion Inhibits CXCR4 Dynamics and CXCL12-Mediated Directed Cell Migration in Human T Cells. *Front Immunol* **13** https://doi.org/10.3389/fimmu.2022.925559 | PubMed

32. **Mañes S.,** et al. (2000) Membrane raft microdomains mediate lateral assemblies required for HIV-1 infection. *EMBO Rep* **1**:190-196 https://doi.org/10.1093/embo-reports/kvd025 | PubMed

33. **Martínez-Muñoz L.,** et al. (2018) Separating Actin-Dependent Chemokine Receptor Nanoclustering from Dimerization Indicates a Role for Clustering in CXCR4 Signaling and Function. *Mol Cell* **70**:106-119.e10 https://doi.org/10.1016/j.molcel.2018.02.034 | PubMed

34. **Del Real G.,** et al. (2002) Blocking of HIV-1 infection by targeting CD4 to nonraft membrane domains. *J Exp Med* **196**:293-301 https://doi.org/10.1084/jem.20020308 | PubMed

35. **Carrasco Y. R.,** Fleire S. J., Cameron T., Dustin M. L., Batista F. D. (2004) LFA- 1/ICAM-1 interaction lowers the threshold of B cell activation by facilitating B cell adhesion and synapse formation. *Immunity* **20**:589-599 https://doi.org/10.1016/s1074-7613(04)00105-0 | PubMed

36. **Martínez Muñoz L.,** et al. (2009) Dynamic regulation of CXCR1 and CXCR2 homo- and heterodimers. *J Immunol* **183**:7337-7346 https://doi.org/10.4049/jimmunol.0901802 | PubMed

37. **Jaqaman K.,** et al. (2008) Robust single-particle tracking in live-cell time-lapse sequences. *Nat Methods* **5**:695-702 https://doi.org/10.1038/nmeth.1237 | PubMed

38. **Dorsch S.,** Klotz K. N., Engelhardt S., Lohse M. J., Bünemann M. (2009) Analysis of receptor oligomerization by FRAP microscopy. *Nat Methods* **6**:225-230 https://doi.org/10.1038/nmeth.1304 | PubMed

39. **Balabanian K.,** et al. (2004) CXCR4-Tropic HIV-1 Envelope Glycoprotein Functions as a Viral Chemokine in Unstimulated Primary CD4 + T Lymphocyteskk. *The Journal of Immunology* **173**:7150-7160 https://doi.org/10.4049/jimmunol.173.12.7150 | PubMed

40. **Arthos J.,** et al. (2000) CCR5 signal transduction in macrophages by human immunodeficiency virus and simian immunodeficiency virus envelopes. *J Virol* **74**:6418-6424 https://doi.org/10.1128/jvi.74.14.6418-6424.2000 | PubMed

41. **Briand G.,** Barbeau B., Tremblay M. (1997) Binding of HIV-1 to its receptor induces tyrosine phosphorylation of several CD4-associated proteins, including the phosphatidylinositol 3-kinase. *Virology* **228**:171-179 https://doi.org/10.1006/viro.1996.8399 | PubMed

42. **Curnock A. P.,** Logan M. K., Ward S. G. (2002) Chemokine signalling: pivoting around multiple phosphoinositide 3-kinases. *Immunology* **105**:125-136 https://doi.org/10.1046/j.1365-2567.2002.01345.x | PubMed

43. **Yoder A.,** et al. (2008) HIV Envelope-CXCR4 Signaling Activates Cofilin to Overcome Cortical Actin Restriction in Resting CD4 T Cells. *Cell* **134**:782-792 https://doi.org/10.1016/j.cell.2008.06.036 | PubMed

44. **Iyengar S.,** Hildreth J. E. K., Schwartz D. H. (1998) Actin-dependent receptor colocalization required for human immunodeficiency virus entry into host cells. *J Virol* **72**:5251-5255 https://doi.org/10.1128/jvi.72.6.5251-5255.1998 | PubMed

45. **Bukrinskaya A. G.** (2004) HIV-1 assembly and maturation. *Arch Virol* **149**:1067-1082 https://doi.org/10.1007/s00705-003-0281-8 | PubMed

46. **Plowman S. J.,** Muncke C., Parton R. G., Hancock J. F. (2005) H-ras, K-ras, and inner plasma membrane raft proteins operate in nanoclusters with differential dependence on the actin cytoskeleton. *Proc Natl Acad Sci U S A* **102**:15500-15505 https://doi.org/10.1073/pnas.0504114102 | PubMed

47. **Torreno-Pina J. A.,** et al. (2016) The actin cytoskeleton modulates the activation of iNKT cells by segregating CD1d nanoclusters on antigen-presenting cells. *Proc Natl Acad Sci U S A* **113**:E772-E781 https://doi.org/10.1073/pnas.1514530113 | PubMed

48. **Pereira P. M.,** et al. (2019) Fix Your Membrane Receptor Imaging: Actin Cytoskeleton and CD4 Membrane Organization Disruption by Chemical Fixation. *Front Immunol* **10** https://doi.org/10.3389/fimmu.2019.00675 | PubMed

49. **Manzo C.,** Garcia-Parajo M. F. (2015) A review of progress in single particle tracking: From methods to biophysical insights. *Reports on Progress in Physics* PubMed | https://doi.org/10.1088/0034-4885/78/12/124601

50. **Ewers H.,** et al. (2005) Single-particle tracking of murine polyoma virus-like particles on live cells and artificial membranes. *Proc Natl Acad Sci U S A* **102**:15110-15115 https://doi.org/10.1073/pnas.0504407102 | PubMed

51. **Calebiro D.,** et al. (2013) Single-molecule analysis of fluorescently labeled G-protein- coupled receptors reveals complexes with distinct dynamics and organization. *Proc Natl Acad Sci U S A* **110**:743-748 https://doi.org/10.1073/pnas.1205798110 | PubMed

52. **Chojnacki J.,** et al. (2017) Envelope glycoprotein mobility on HIV-1 particles depends on the virus maturation state. *Nat Commun* **8** https://doi.org/10.1038/s41467-017-00515-6 | PubMed

53. **Hart T. K.,** Klinkner A. M., Ventre J., Bugelski P. J. (1993) Morphometric analysis of envelope glycoprotein gp120 distribution on HIV-1 virions. *J Histochem Cytochem* **41**:265-271 https://doi.org/10.1177/41.2.7678271 | PubMed

54. **Zhu P.,** et al. (2003) Electron tomography analysis of envelope glycoprotein trimers on HIV and simian immunodeficiency virus virions. *Proc Natl Acad Sci U S A* **100**:15812-15817 https://doi.org/10.1073/pnas.2634931100 | PubMed

55. **Zhu P.,** et al. (2006) Distribution and three-dimensional structure of AIDS virus envelope spikes. *Nature* **441**:847-852 https://doi.org/10.1038/nature04817 | PubMed

56. **Murakami T.,** Ablan S., Freed E. O., Tanaka Y. (2004) Regulation of human immunodeficiency virus type 1 Env-mediated membrane fusion by viral protease activity. *J Virol* **78**:1026-1031 https://doi.org/10.1128/jvi.78.2.1026-1031.2004 | PubMed

57. **Wyma D. J.,** et al. (2004) Coupling of human immunodeficiency virus type 1 fusion to virion maturation: a novel role of the gp41 cytoplasmic tail. *J Virol* **78**:3429-3435 https://doi.org/10.1128/jvi.78.7.3429-3435.2004 | PubMed

58. **Rauh N. R.,** Schmidt A., Bormann J., Nigg E. A., Mayer T. U. (2005) Calcium triggers exit from meiosis II by targeting the APC/C inhibitor XErp1 for degradation. *Nature* **437**:1048-1052 https://doi.org/10.1038/nature04093 | PubMed

59. **Balabanian K.,** et al. (2005) WHIM syndromes with different genetic anomalies are accounted for by impaired CXCR4 desensitization to CXCL12. *Blood* **105**:2449-2457 https://doi.org/10.1182/blood-2004-06-2289 | PubMed

60. **Hernandez P. A.,** et al. (2003) Mutations in the chemokine receptor gene CXCR4 are associated with WHIM syndrome, a combined immunodeficiency disease. *Nat Genet* **34**:70-74 https://doi.org/10.1038/ng1149 | PubMed

61. **Busillo J. M.,** Benovic J. L. (2007) Regulation of CXCR4 signaling. *Biochim Biophys Acta* **1768**:952-963 https://doi.org/10.1016/j.bbamem.2006.11.002 | PubMed

62. **Mcdermott D. H.,** et al. (2011) AMD3100 is a potent antagonist at CXCR4(R334X), a hyperfunctional mutant chemokine receptor and cause of WHIM syndrome. *J Cell Mol Med* **15**:2071-2081 https://doi.org/10.1111/j.1582-4934.2010.01210.x | PubMed

63. **Singer I. I.,** et al. (2001) CCR5, CXCR4, and CD4 are clustered and closely apposed on microvilli of human macrophages and T cells. *J Virol* **75**:3779-3790 https://doi.org/10.1128/jvi.75.8.3779-3790.2001 | PubMed

64. **Abramson J.,** et al. (2024) Accurate structure prediction of biomolecular interactions with AlphaFold 3. *Nature* **630**:493-500 https://doi.org/10.1038/s41586-024-07487-w | PubMed

65. **Basmaciogullari S.,** Pacheco B., Bour S., Sodroski J. (2006) Specific interaction of CXCR4 with CD4 and CD8alpha: functional analysis of the CD4/CXCR4 interaction in the context of HIV-1 envelope glycoprotein-mediated membrane fusion. *Virology* **353**:52-67 https://doi.org/10.1016/j.virol.2006.05.027 | PubMed

66. **Zaitseva M.,** et al. (2005) Increased CXCR4-dependent HIV-1 fusion in activated T cells: role of CD4/CXCR4 association. *J Leukoc Biol* **78**:1306-1317 https://doi.org/10.1189/jlb.0105043 | PubMed

67. **Lapham C. K.,** Zaitseva M. B., Lee S., Romanstseva T., Golding H. (1999) Fusion of monocytes and macrophages with HIV-1 correlates with biochemical properties of CXCR4 and CCR5. *Nat Med* **5**:303-308 https://doi.org/10.1038/6523 | PubMed

68. **Lee S.,** et al. (2000) Coreceptor competition for association with CD4 may change the susceptibility of human cells to infection with T-tropic and macrophagetropic isolates of human immunodeficiency virus type 1. *J Virol* **74**:5016-5023 https://doi.org/10.1128/jvi.74.11.5016-5023.2000 | PubMed

69. **Hoxie J. A.,** et al. (1986) Alterations in T4 (CD4) protein and mRNA synthesis in cells infected with HIV. *Science* **234**:1123-1127 https://doi.org/10.1126/science.3095925 | PubMed

70. **Potash** (1998) Viral interference in HIV-1 infected cells. *Reviews in Medical Virology* https://doi.org/10.1002/(sici)1099-1654(1998100)8:4<203::aid-rmv224>3.0.co;2-# | PubMed

71. **Chenine A. L.,** Sattentau Q., Moulard M. (2000) Selective HIV-1-induced downmodulation of CD4 and coreceptors. *Arch Virol* **145**:455-471 https://doi.org/10.1007/s007050050039 | PubMed

72. **Choi B.,** et al. (2008) Down-regulation of cell surface CXCR4 by HIV-1. *Virol J* **5** https://doi.org/10.1186/1743-422x-5-6 | PubMed

73. **Balabanian K.,** Lagane B., J. Pablos L. L. (2005) WHIM syndromes with different genetic anomalies are accounted for by impaired CXCR4 desensitization to CXCL12. *Blood* https://doi.org/10.1182/blood-2004-06-2289 | PubMed

74. **Wyatt R.,** Sodroski J. (1998) The HIV-1 envelope glycoproteins: fusogens, antigens, and immunogens. *Science* **280**:1884-1888 https://doi.org/10.1126/science.280.5371.1884 | PubMed

75. **Blumenthal R.,** Durell S., Viard M. (2012) HIV entry and envelope glycoprotein- mediated fusion. *J Biol Chem* **287**:40841-40849 https://doi.org/10.1074/jbc.r112.406272 | PubMed

76. **Chen B.** (2019) Molecular Mechanism of HIV-1 Entry. *Trends Microbiol* **27**:878-891 https://doi.org/10.1016/j.tim.2019.06.002 | PubMed

77. **Traunecker A.,** Schneider J., Kiefer H., Karjalainen K. (1989) Highly efficient neutralization of HIV with recombinant CD4-immunoglobulin molecules. *Nature* **339**:68-70 https://doi.org/10.1038/339068a0 | PubMed

78. **Nara P. L.,** Hwang K. M., Rausch D. M., Lifson J. D., Eiden L. E. (1989) CD4 antigen- based antireceptor peptides inhibit infectivity of human immunodeficiency virus in vitro at multiple stages of the viral life cycle. *Proc Natl Acad Sci U S A* **86**:7139-7143 https://doi.org/10.1073/pnas.86.18.7139 | PubMed

79. **Schooley R. T.,** et al. (1990) Recombinant soluble CD4 therapy in patients with the acquired immunodeficiency syndrome (AIDS) and AIDS-related complex. A phase I-II escalating dosage trial. *Ann Intern Med* **112**:247-253 https://doi.org/10.7326/0003-4819-112-4-247 | PubMed

80. **Kahn J. O.,** et al. (1990) The safety and pharmacokinetics of recombinant soluble CD4 (rCD4) in subjects with the acquired immunodeficiency syndrome (AIDS) and AIDS-related complex. A phase 1 study. *Ann Intern Med* **112**:254-261 https://doi.org/10.7326/0003-4819-112-4- | PubMed

81. **Hoffmann M. A. G.,** et al. (2020) Nanoparticles presenting clusters of CD4 expose a universal vulnerability of HIV-1 by mimicking target cells. *Proc Natl Acad Sci U S A* **117**:18719-18728 https://doi.org/10.1073/pnas.2010320117 | PubMed

82. **Schamel W. W. A.,** Alarcón B. (2013) Organization of the resting TCR in nanoscale oligomers. *Immunol Rev* **251**:13-20 https://doi.org/10.1111/imr.12019 | PubMed

83. **Razvag Y.,** et al. (2019) T Cell Activation through Isolated Tight Contacts. *Cell Rep* **29**:3506-3521.e6 https://doi.org/10.1016/j.celrep.2019.11.022 | PubMed

84. **Lillemeier B. F.,** et al. (2010) TCR and Lat are expressed on separate protein islands on T cell membranes and concatenate during activation. *Nat Immunol* **11**:90-96 https://doi.org/10.1038/ni.1832 | PubMed

85. **Verstreken P.,** Bellen H. J. (2002) Meaningless minis? Mechanisms of neurotransmitter- receptor clustering. *Trends Neurosci* **25**:383-385 https://doi.org/10.1016/s0166-2236(02)02197-5 | PubMed

86. **Germain R. N.** (1997) T-cell signaling: the importance of receptor clustering. *Curr Biol* **7** https://doi.org/10.1016/s0960-9822(06)00323-x | PubMed

87. **Cairo C. W.** (2007) Signaling by committee: receptor clusters determine pathways of cellular activation. *ACS Chem Biol* **2**:652-655 https://doi.org/10.1021/cb700214x | PubMed

88. **Chang M. I.,** Panorchan P., Dobrowsky T. M., Tseng Y., Wirtz D. (2005) Single- molecule analysis of human immunodeficiency virus type 1 gp120-receptor interactions in living cells. *J Virol* **79**:14748-14755 https://doi.org/10.1128/jvi.79.23.14748-14755.2005 | PubMed

89. **Bray D.** (1995) Protein molecules as computational elements in living cells. *Nature* **376**:307-312 https://doi.org/10.1038/376307a0 | PubMed

90. **Cho W.,** Stahelin R. V. (2005) Membrane-protein interactions in cell signaling and membrane trafficking. *Annu Rev Biophys Biomol Struct* **34**:119-151 https://doi.org/10.1146/annurev.biophys.33.110502.133337 | PubMed

91. **Gurry T.,** Kahramanoğullari O., Endres R. G. (2009) Biophysical mechanism for ras- nanocluster formation and signaling in plasma membrane. *PLoS One* **4** https://doi.org/10.1371/journal.pone.0006148 | PubMed

92. **Popik W.,** Hesselgesser J. E., Pitha P. M. (1998) Binding of human immunodeficiency virus type 1 to CD4 and CXCR4 receptors differentially regulates expression of inflammatory genes and activates the MEK/ERK signaling pathway. *J Virol* **72**:6406-6413 https://doi.org/10.1128/jvi.72.8.6406-6413.1998 | PubMed

93. **Davis C. B.,** et al. (1997) Signal transduction due to HIV-1 envelope interactions with chemokine receptors CXCR4 or CCR5. *J Exp Med* **186**:1793-1798 https://doi.org/10.1084/jem.186.10.1793 | PubMed

94. **Pasquereau S.,** Herbein G. (2022) CounterAKTing HIV: Toward a "Block and Clear" Strategy?. *Front Cell Infect Microbiol* **12** https://doi.org/10.3389/fcimb.2022.827717 | PubMed

95. **François F.,** Klotman M. E. (2003) Phosphatidylinositol 3-kinase regulates human immunodeficiency virus type 1 replication following viral entry in primary CD4+ T lymphocytes and macrophages. *J Virol* **77**:2539-2549 https://doi.org/10.1128/jvi.77.4.2539-2549.2003 | PubMed

96. **Deng J.,** et al. (2016) HIV Envelope gp120 Alters T Cell Receptor Mobilization in the Immunological Synapse of Uninfected CD4 T Cells and Augments T Cell Activation. *J Virol* **90**:10513-10526 https://doi.org/10.1128/jvi.01532-16 | PubMed

97. **Chertova E.,** et al. (2002) Envelope glycoprotein incorporation, not shedding of surface envelope glycoprotein (gp120/SU), Is the primary determinant of SU content of purified human immunodeficiency virus type 1 and simian immunodeficiency virus. *J Virol* **76**:5315-5325 https://doi.org/10.1128/jvi.76.11.5315-5325.2002 | PubMed

98. **DeSantis M. C.,** Kim J. H., Song H., Klasse P. J., Cheng W. (2016) Quantitative Correlation between Infectivity and Gp120 Density on HIV-1 Virions Revealed by Optical Trapping Virometry. *J Biol Chem* **291**:13088-13097 https://doi.org/10.1074/jbc.m116.729210 | PubMed

99. **García-Cuesta E. M.,** et al. (2024) Allosteric modulation of the CXCR4:CXCL12 axis by targeting receptor nanoclustering via the TMV-TMVI domain. *eLife* **13** https://doi.org/10.7554/elife.93968 | PubMed

100. **Kumar R.,** et al. (2023) Reduced G protein signaling despite impaired internalization and β-arrestin recruitment in patients carrying a CXCR4Leu317fsX3 mutation causing WHIM syndrome. *JCI Insight* **8** https://doi.org/10.1172/jci.insight.145688 | PubMed

101. **Geleziunas R.,** Bour S., Wainberg M. A. (1994) Cell surface down-modulation of CD4 after infection by HIV-1. *FASEB J* **8**:593-600 https://doi.org/10.1096/fasebj.8.9.8005387 | PubMed

102. **Hubert P.,** Bismuth G., Körner M., Debré P. (1995) HIV-1 glycoprotein gp120 disrupts CD4-p56lck/CD3-T cell receptor interactions and inhibits CD3 signaling. *Eur J Immunol* **25**:1417-1425 https://doi.org/10.1002/eji.1830250542 | PubMed

103. **Daecke J.,** Fackler O. T., Dittmar M. T., Kräusslich H.-G. (2005) Involvement of clathrin-mediated endocytosis in human immunodeficiency virus type 1 entry. *J Virol* **79**:1581-1594 https://doi.org/10.1128/jvi.79.3.1581-1594.2005 | PubMed

104. **Aggarwal A.,** et al. (2017) HIV infection is influenced by dynamin at 3 independent points in the viral life cycle. *Traffic* **18**:392-410 https://doi.org/10.1111/tra.12481 | PubMed

105. **de la Vega M.,** et al. (2011) Inhibition of HIV-1 endocytosis allows lipid mixing at the plasma membrane, but not complete fusion. *Retrovirology* **8**:99 https://doi.org/10.1186/1742-4690-8-99 | PubMed

106. **Miyauchi K.,** Kim Y., Latinovic O., Morozov V., Melikyan G. B. (2009) HIV enters cells via endocytosis and dynamin-dependent fusion with endosomes. *Cell* **137**:433-444 https://doi.org/10.1016/j.cell.2009.02.046 | PubMed

107. **Carter G. C.,** Bernstone L., Baskaran D., James W. (2011) HIV-1 infects macrophages by exploiting an endocytic route dependent on dynamin, Rac1 and Pak1. *Virology* **409**:234-250 https://doi.org/10.1016/j.virol.2010.10.018 | PubMed

108. **Van Wilgenburg B.,** Moore M. D., James W. S., Cowley S. A. (2014) The productive entry pathway of HIV-1 in macrophages is dependent on endocytosis through lipid rafts containing CD4. *PLoS One* **9** https://doi.org/10.1371/journal.pone.0086071 | PubMed

109. **Toyoda M.,** et al. (2015) Differential Ability of Primary HIV-1 Nef Isolates To Downregulate HIV-1 Entry Receptors. *J Virol* **89**:9639-9652 https://doi.org/10.1128/jvi.01548-15 | PubMed

110. **Venzke S.,** Michel N., Allespach I., Fackler O. T., Keppler O. T. (2006) Expression of Nef downregulates CXCR4, the major coreceptor of human immunodeficiency virus, from the surfaces of target cells and thereby enhances resistance to superinfection. *J Virol* **80**:11141-11152 https://doi.org/10.1128/jvi.01556-06 | PubMed

111. **Gobeil L.-A.,** Lodge R., Tremblay M. J. (2013) Macropinocytosis-like HIV-1 internalization in macrophages is CCR5 dependent and leads to efficient but delayed degradation in endosomal compartments. *J Virol* **87**:735-745 https://doi.org/10.1128/jvi.01802-12 | PubMed

112. **Popik W.,** Alce T. M., Au W.-C. (2002) Human immunodeficiency virus type 1 uses lipid raft-colocalized CD4 and chemokine receptors for productive entry into CD4(+) T cells. *J Virol* **76**:4709-4722 https://doi.org/10.1128/jvi.76.10.4709-4722.2002 | PubMed

113. **Neel N. F.,** Schutyser E., Sai J., Fan G. H., Richmond A. (2005) Chemokine receptor internalization and intracellular trafficking. *Cytokine Growth Factor Rev* **16**:637-658 https://doi.org/10.1016/j.cytogfr.2005.05.008 | PubMed

114. **Gardeta S. R.,** et al. (2022) Sphingomyelin Depletion Inhibits CXCR4 Dynamics and CXCL12-Mediated Directed Cell Migration in Human T Cells. *Front Immunol* **13** https://doi.org/10.3389/fimmu.2022.925559 | PubMed

115. **Hauser M. A.,** et al. (2016) Inflammation-Induced CCR7 Oligomers Form Scaffolds to Integrate Distinct Signaling Pathways for Efficient Cell Migration. *Immunity* **44**:59-72 https://doi.org/10.1016/j.immuni.2015.12.010 | PubMed

116. **Harrop H. A.,** Rider C. C. (1998) Heparin and its derivatives bind to HIV-1 recombinant envelope glycoproteins, rather than to recombinant HIV-1 receptor, CD4. *Glycobiology* **8**:131-137 https://doi.org/10.1093/glycob/8.2.131 | PubMed

117. **Mondor I.,** Ugolini S., Sattentau Q. J. (1998) Human immunodeficiency virus type 1 attachment to HeLa CD4 cells is CD4 independent and gp120 dependent and requires cell surface heparans. *J Virol* **72**:3623-3634 https://doi.org/10.1128/jvi.72.5.3623-3634.1998 | PubMed

118. **Saphire A. C. S.,** Bobardt M. D., Zhang Z., David G., Gallay P. A. (2001) Syndecans serve as attachment receptors for human immunodeficiency virus type 1 on macrophages. *J Virol* **75**:9187-9200 https://doi.org/10.1128/jvi.75.19.9187-9200.2001 | PubMed

119. **Moulard M.,** et al. (2000) Selective interactions of polyanions with basic surfaces on human immunodeficiency virus type 1 gp120. *J Virol* **74**:1948-1960 https://doi.org/10.1128/jvi.74.4.1948-1960.2000 | PubMed

120. **Ugolini S.,** Mondor I., Sattentau Q. J. (1999) HIV-1 attachment: another look. *Trends Microbiol* **7**:144-149 https://doi.org/10.1016/s0966-842x(99)01474-2 | PubMed

121. **Dobrowsky T. M.,** Zhou Y., Sun S. X., Siliciano R. F., Wirtz D. (2008) Monitoring early fusion dynamics of human immunodeficiency virus type 1 at single-molecule resolution. *J Virol* **82**:7022-7033 https://doi.org/10.1128/jvi.00053-08 | PubMed

122. **Rabenstein D. L.** (2002) Heparin and heparan sulfate: structure and function. *Nat Prod Rep* **19**:312-331 https://doi.org/10.1039/b100916h | PubMed

123. **Cambi A.,** et al. (2004) Microdomains of the C-type lectin DC-SIGN are portals for virus entry into dendritic cells. *J Cell Biol* **164**:145-155 https://doi.org/10.1083/jcb.200306112 | PubMed

124. **Wu L.,** KewalRamani V. N. (2006) Dendritic-cell interactions with HIV: infection and viral dissemination. *Nat Rev Immunol* **6**:859-868 https://doi.org/10.1038/nri1960 | PubMed

# Peer reviews

## Reviewer #1 (Public review):

Summary:

This article provides new insights into the organisational changes of the X4-tropic HIV-1 co-receptor CXCR4 upon binding of the viral receptor-binding protein X4-gp120, either in its soluble form or when displayed as Env on virus-like particles (VLPs). The study employs single-particle tracking total internal reflection fluorescence (SPT-TIRF) microscopy to quantify the dynamics and clustering of CXCR4 on CD4+ T cells. The data show that CXCR4 clusters in the presence of X4-gp120 and VLPs, a phenomenon that is also observed for the primary HIV-1 receptor CD4. The authors also show that a WHIM mutant of CXCR4 (CXCR4-R334X) that does not cluster in the presence of its natural ligand, CXCL12, clusters in the presence of X4-gp120 and VLPs.

Major strengths:

The data are well presented, discussed, and supported by solid evidence. Literature is cited appropriately.

Major weaknesses:

The authors have addressed my concerns in the revised manuscript.

Significance:

In summary, the work is presented in a clear fashion, and the main findings are properly highlighted. The paper will be of interest to the broader virology community as well as to researchers studying cell receptor clustering. The findings are not entirely surprising because it has been shown previously that the binding of Env to CD4 mediates CD4 clustering, which would also suggest clustering of the co-receptor. Nonetheless, the paper provides strong evidence that CXCR4 clusters and changes its dynamics in the presence of CD4 and X4-gp120. Moreover, the evidence that X4-gp120 clusters CXCR4-R334X is of high interest as it suggests a different binding mechanism for X4-gp120 from that of the natural ligand CXCL12, raising questions for further research.

https://doi.org/10.7554/eLife.110354.1.sa4

## Reviewer #2 (Public review):

Summary:

The author investigates how the HIV-1 Env glycoprotein modulates the nanoscale organisation and dynamics of the CXCR4 co-receptor on $CD4^+$ T cells. The author demonstrates that HIV-1 Env induces CXCR4 clustering distinct from that triggered by its natural ligand (CXCL12), implicating spatial receptor organization as a determinant of infection. This study investigates how HIV-1 Env (specifically X4-tropic gp120) alters the membrane organization and dynamics of the chemokine receptor CXCR4 and its WHIM-associated mutant, CXCR4R334X, in a CD4-dependent manner. Using single-particle tracking total internal reflection fluorescence microscopy (SPT-TIRF-M), the authors demonstrate that both soluble gp120 and virus-like particles (VLPs) displaying gp120 induce CXCR4 nanoclustering, reduce receptor diffusivity, and promote immobile nanoclusters of CXCR4 at the membrane of Jurkat T cells and primary $CD4^+$ T cell blasts. The work offers new insights into the spatial organisation of receptors during HIV-1 entry and infection. The manuscript is well-written, and the findings are significant.

Significance:

Nature and significance of the advance:

This work marks a conceptual and mechanistic breakthrough in understanding HIV-1 entry. It goes beyond the static view of Env-co-receptor interaction to show that nanoscale reorganization of CXCR4, distinct from chemokine-induced clustering, occurs during HIV-1 Env engagement and may be essential for infection.

Context within existing literature. Previous studies established Env-induced CD4 clustering (Yin et al., 2020) and chemokine-induced CXCR4 nanocluster formation (Martínez-Muñoz et al., 2018), but the exact nanoscale rearrangement of CXCR4 in the context of HIV-1 Env and physiological Env densities remains unquantified. This study addresses this gap using SPT-TIRF, STED microscopy, and functional assays.

Audience and influence: The findings will be of interest to researchers in HIV virology, membrane receptor biology, viral entry mechanisms, and therapeutic target development. The receptor-clustering aspect could also influence broader fields of study, such as GPCR organization and immune receptor signalling.

Reviewer expertise: I can evaluate HIV-1 entry mechanisms, viral glycoprotein-host-host-host receptor interactions, single-molecule fluorescence microscopy, and membrane protein dynamics. I am less equipped to evaluate the deep structural modelling aspects, though the in silico AlphaFold results are straightforward to interpret in context.

https://doi.org/10.7554/eLife.110354.1.sa3

## Reviewer #3 (Public review):

Summary:

The authors investigate how HIV-1 Env engagement affects the nanoscale organization and dynamics of the CXCR4 coreceptor on target cells. Using single-particle tracking TIRF microscopy, they analyze CXCR4 distribution following exposure to gp120 or HIV virus-like particles, including both wild-type CXCR4 and the WHIM-associated CXCR4.R334X variant. The study further examines the role of CD4-CXCR4 heterodimerization and contrasts Env-induced receptor organization with that elicited by the natural ligand CXCL12.

Evaluation:

A major strength of this work is the integration of high-resolution imaging with functional and comparative analyses that distinguish Env-induced CXCR4 clustering from chemokine-driven effects. The experiments are clearly described, include appropriate controls, and are supported by quantitative analyses that are consistent across experiments. The revised manuscript appears to have addressed many of the technical and interpretive issues raised during initial review, improving clarity around data analysis and strengthening confidence in the conclusions.

I am not an expert in TIRF microscopy or single-molecule tracking and defer to other reviewers regarding limits of imaging and tracking methods. However, I did not identify major inconsistencies between the biological data presented and the conclusions drawn.

The authors data support the conclusion that HIV-1 Env, delivered as gp120 or virus-like particles, promotes CD4-dependent nanoscale clustering of CXCR4, including the CXCR4.R334X variant associated with WHIM syndrome, in a manner distinct from CXCL12-induced receptor organization. The authors are generally careful to frame their conclusions in proportion to the evidence and avoid overinterpretation.

Overall, this study builds on prior work on CXCR4 distribution and HIV entry by providing higher-resolution insight into receptor nanoclustering and its modulation by Env. The findings provide a mechanistic refinement rather than a conceptual paradigm shift but is a valuable dataset useful to researchers studying HIV entry, coreceptor biology, and membrane receptor organization.

Reviewer expertise: HIV-1 Envelope glycoproteins and entry assays, HIV broadly neutralizing antibodies, HIV vaccine design

Comments on revised version:

This reviewer has no further recommendations and thanks the authors for clarifying that the Env content in gp120-VLPs was lower than the NL4-3deltaIN particles but that the percentage of mature particles in the gp120-VLPs was higher.

https://doi.org/10.7554/eLife.110354.1.sa2

## Reviewer #4 (Public review):

Summary:

The authors investigate the impact of surface bound HIV gp120 and VLPs on CXCR4 dynamics in Jurkat T cells expressing WT or WHIM syndrome mutated CXCR4, which has a defective response to CXCL12. Jurkat cells were transfected with CXCR4-AcGFP. Images were acquired and a single particle tracking routine was applied to generate information about nanoclustering and diffusion, and FRET was used to investigate CD4-CXCR4 proximity. They compare effects of soluble gp120 to immature and mature VLPs, which include varying degrees of gp120 clustering. They find that solid phase gp120 or VLP can increase CXCR4 clustering size and decrease diffusion in Jurkat cells. Surprisingly, VLP lacking gp120 could increase CXCR4 clustering and speed, which is paradoxical as there were no known ligands on the VLPs, but they likely carry many cellular proteins with potential interactions. The impact of CXCL12 and gp120 binding to CXCR4 was different in terms of clustering and receptor down-regulation.

Significance:

The strengths are that it's an important question and the reagents are well prepared and characterised. They are detecting quantitative effects that will likely be reproducible. The information generated is potentially useful for those studying HIV infection processes and strategies to prevent infection.

The major weakness is that the conditions for the SPT experiments are not ideal in that the density of particles is too high for SPT and the single molecule basis for assessing nanoclusters is not clear. This means that the data is getting at complex molecules phenomena and less likely be generating pure single molecules measurements.

Comments on revised version:

The authors should make the tracking data available and this will aid others in following up on it.

https://doi.org/10.7554/eLife.110354.1.sa1

## Author response:

> ***Point-by-point description of the revisions***

> ***Reviewer #1:***

Thank you very much for considering that our manuscript evaluates an important question and that the reagents used are well prepared and characterized. We also much appreciate that you consider the information generated as potentially useful for those studying HIV infection processes and strategies to prevent infection.

> *(1) While a single particle tracking routine was applied to the data, it's not clear how the signal from a single GFP was defined and if movement during the 100 ms acquisition time impacts this. My concern would be that the routine is tracking fluctuations, and these are related to single particle dynamics, it appears from the movies that the density or the GFP tagged receptors in the cells is too high to allow clear tracking of single molecules. SPT with GFP is very difficult due to bleaching and relatively low quantum yield. Current efforts in this direction that are more successful include using SNAP tags with very photostable organic fluorophores. The data likely does mean something is happening with the receptor, but they need to be more conservative about the interpretation.*
>
> *Some of the paradoxical effects might be better understood through deeper analysis of the SPT data, particularly investigation of active transport and more detailed analysis of "immobile" objects. Comments on early figures illustrate how this could be approached. This would require selecting acquisitions where the GFP density is low enough for SPT and performing a more detailed analysis, but this may be difficult to do with GFP.*
>
> *When the authors discuss clusters of <2 or >3, how do they calibrate the value of GFP and the impact of diffusion on the measurement. One way to approach this might be single molecules measurements of dilute samples on glass vs in a supported lipid bilayer to map the streams of true immobility to diffusion at >1 μm2/sec.*

We fully understand the reviewer's apprehensions regarding the application of these high-end biophysical techniques, in particular the associated complexity of the data analysis. We provide below extensive explanations on our methodology, which we hope will satisfactorily address all of the reviewer's concerns.

We would first like to emphasize that the experimental conditions and the quantitative analysis used in our current experiments are similar to the established protocols and methodologies applied by our group previously (Martinez-Muñoz et al. Mol. Cell, 2018; García-Cuesta et al. PNAS, 2022; Gardeta et al. Frontiers in Immunol., 2022; García-Cuesta et al. eLife, 2024; Gardeta et al. Cell. Commun. Signal., 2025) and by others (Calebiro et al. PNAS, 2013; Jaqaman et al. Cell, 2011; Mattila et al. Immunity, 2013; Torreno-Pina et al. PNAS, 2014; Torreno-Pina et al. PNAS, 2016).

As SPT (single-particle tracking) experiments require low-expressing conditions in order to follow individual trajectories (Manzo & García-Parajo Rep. Prog. Phys., 2015), we transiently transfected Jurkat $CD4^+$ cells with CXCR4-AcGFP or $CXCR4^{R334X}$-AcGFP. At 24 h post-transfection, cells expressing low CXCR4-AcGFP levels were selected by a MoFlo Astrios Cell Sorter (BeckmanCoulter) to ensure optimal conditions for SPT. Using Dako Qifikit (DakoCytomation), we quantified the number of CXCR4 receptors and found ~8,500 – 22,000 CXCR4-AcGFP receptors/cell, which correspond to a particle density ~2 – 4.5 particles/$\mu m^2$ (Author response image 1) and are similar to the expression levels found in primary human lymphocytes.

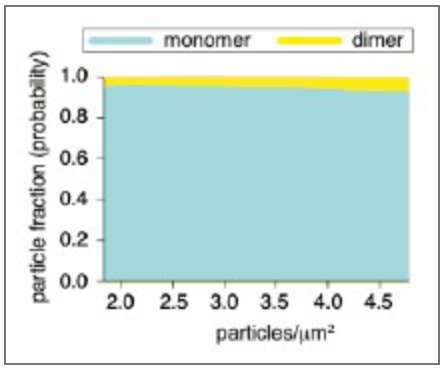


**Author response image 1. Purified AcGFP monomeric protein was immobilized on glass at various concentrations.** Dependency of the distribution of particle components on particle density was calculated; >95% were monomeric single particles at 2.0-4.5 particles/μm$^2$. This range of particle density was used to analyze the dynamics of CXCR4-AcGFP, or CXCR4$^{R334X}$-AcGFP single particles on JKCD4 cells.

These cells were resuspended in RPMI supplemented with 2% FBS, NaPyr and L-glutamine and plated on 96-well plates for at least 2 h. Cells were centrifuged and resuspended in a buffer with HBSS, 25 mM HEPES, 2% FBS (pH 7.3) and plated on glass-bottomed microwell dishes (MatTek Corp.) coated with fibronectin (FN) (Sigma-Aldrich, 20 μg/ml, 1 h, 37°C). To observe the effect of the ligand, we coated dishes with FN + CXCL12; FN + X4-gp120 or FN + VLPs, as described in material and methods; cells were incubated (20 min, 37°C, 5% $CO_2$) before image acquisition.

For SPT measurements, we use a total internal reflection fluorescence (TIRF) microscope (Leica AM TIRF inverted) equipped with an EM-CCD camera (Andor DU 885-CS0-#10-VP), a 100x oilimmersion objective (HCX PL APO 100x/1.46 NA) and a 488-nm diode laser. The microscope was equipped with incubator and temperature control units; experiments were performed at 37°C with 5% $CO_2$. To minimize photobleaching effects before image acquisition, cells were located and focused using the bright field, and a fine focus adjustment in TIRF mode was made at 5% laser power, an intensity insufficient for single-particle detection that ensures negligible photobleaching. Image sequences of individual particles (500 frames) were acquired at 49% laser power with a frame rate of 10 Hz (100 ms/frame). The penetration depth of the evanescent field used was 90 nm.

We performed automatic tracking of individual particles using a very well established and common algorithm first described by Jaqaman (Jaqaman et al. Nat. Methods, 2008). Nevertheless, we would stress that we implemented this algorithm in a supervised fashion, i.e., we visually inspect each individual trajectory reconstruction in a separate window. Indeed, this algorithm is not able to quantify merging or splitting events.

We follow each individual fluorescence spot frame-by-frame using a three-by-three matrix around the centroid position of the spot, as it diffuses on the cell membrane. To minimize the effect of photon fluctuations, we averaged the intensity over 20 frames. Nevertheless, to assure the reviewer that most of the single molecule traces last for at least 50 frames (i.e., 5 seconds), we provide the following data and arguments. We currently measure the photobleaching times from individual CD86-AcGFP spots exclusively having one single photobleaching step to guarantee that we are looking at individual CD86-AcGFP molecules. The distribution of the photobleaching times is shown below (Author response image 2). Fitting of the distribution to a single exponential decay renders a t0 value of ~5 s. Thus, with 20 frames averaging, we are essentially measuring the whole population of monomers in our experiments. As the survival time of a molecule before photobleaching will strongly depend on the excitation conditions, we used low excitation conditions (2 mW laser power, which corresponds to an excitation power density of ~0.015 kW/cm$^2$ considering the illumination

region) and longer integration times (100 ms/frame) to increase the signal-to-background for single GFP detection while minimizing photobleaching.

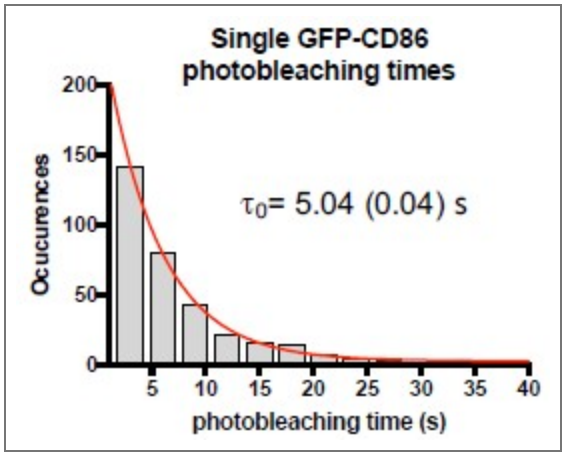


**Author response image 2. Single molecule photobleaching times measured directly from single molecule trajectories of CD86-AcGFP, considering only traces that exhibit single molecule photobleaching steps.** The experimental data are shown in gray bars (n=273 trajectories over 3 independent experiments). The red line corresponds to a single exponential decay fitting of the experimental data, from where $t_o$ has been extracted.

To infer the stoichiometry of receptor complexes, we also perform single-step photobleaching analysis of the TIRF trajectories to establish the existence of different populations of monomers, dimers, trimers and nanoclusters and extract their percentage. Some representative trajectories of CXCR4-AcGFP with the number of steps detected are shown in new Supplementary Figure 1.

The emitted fluorescence (arbitrary units, a.u.) of each spot in the cells is quantified and normalized to the intensity emitted by monomeric CD86-AcGFP spots that strictly showed a single photobleaching step (Dorsch et al. Nat. Methods, 2009). We have preferred to use CD86-AcGFP in cells rather than AcGFP on glass to exclude any potential effect on the different photodynamics exhibited by AcGFP when bound directly to glass. We have also previously shown pharmacological controls to exclude CXCL12-mediated receptor clustering due to internalization processes (Martinez-Muñoz et al. Mol. Cell, 2018) that, together with the evaluation of single photobleaching steps and intensity histograms, allow us to exclude the presence of vesicles in our data. Thus, the dimers, trimers and nanoclusters found in our data do correspond to CXCR4 molecules on the cell surface. Finally, distribution of monomeric particle intensities, obtained from the photobleaching analysis, was analyzed by Gaussian fitting, rendering a mean value of 980 ± 86 a.u. This value was then used as the monomer reference to estimate the number of receptors per particle in both cases, CXCR4-AcGFP and $CXCR4^{R334X}$-AcGFP (new Supplementary Figure 1).

> *(2) I understand that the CXCL12 or gp120 are attached to the substrate with fibronectin for adhesion. I'm less clear how how that VLPs are integrated. Were these added to cells already attached to FN?*

For TIRF-M experiments, cells were adhered to glass-bottomed microwell dishes coated with fibronectin, fibronectin + CXCL12, fibronectin + X4-gp120, or fibronectin + VLPs. As for CXCL12 and X4-gp120, the VLPs were attached to fibronectin taking advantage of electrostatic interactions. To clarify the integration of the VLPs in these assays, we have stained the microwell dishes coated with fibronectin and those coated with fibronectin + VLPs with wheat germ agglutinin (WGA) coupled to Alexa647 (Author response image 3) and evaluated

the staining by confocal microscopy. These results indicate the presence of carbohydrates on the VLPs and are, therefore, indicative of the presence of VLPs on the fibronectin layer.

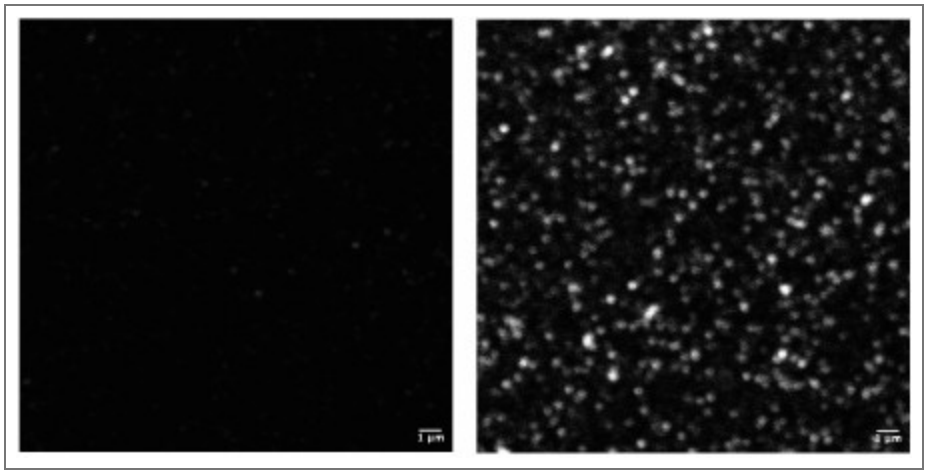

**Author response image 3. Representative confocal images of microwell dishes coated with fibronectin ((left panel) or fibronectin + VLPs (right panel)) and stained with wheat germ agglutinin (WGA) coupled to Alexa647.** Bar scale 1µm.

Moreover, it is important to remark that the effect of the VLPs on CXCR4 behavior at the cell surface observed by TIRF-M confirmed that the VLPs remained attached to the substrate during the experiment.

> *(3) Fig 1A - The classification of particle tracks into mobile and immobile is overly simplistic description that goes back to bulk FRAP measurements and it not really applicable to single molecule tracking data, where it's rare to see anything that is immobile and alive. An alternative classification strategy uses sub-diffusion, normal diffusion and active diffusion (or active transport) to descriptions and particles can transition between these classes over the tracking period. Fig 1B- this data might be better displayed as histograms showing distributions within the different movement classes.*

In agreement with the reviewer's commentary, the majority of the particles detected in our TIRFM experiments were indeed mobile. However, we also detected a variable, and biologically appreciable, percentage of immobile particles depending on the experimental condition analyzed (Figure 1A in the main manuscript). To establish a stringent threshold for identifying these immobile particles under our specific experimental conditions, we used purified monomeric AcGFP proteins immobilized on glass coverslips. Our analysis demonstrated that 95% of these immobilized proteins showed a diffusion coefficient £0.0015 $\mu m^2/s$; consequently, this value was established as the cutoff to distinguish immobile from mobile trajectories. While the observation of truly immobile entities in a dynamic, living system is rare, the presence of these particles under our conditions is biologically significant. For instance, the detection of large, immobile receptor nanoclusters at the plasma membrane is entirely consistent with facilitating key cellular processes, such as enabling the robust signaling cascade triggered by ligand binding or promoting the crucial events required for efficient viral entry into the cells.

Regarding the mobile receptors (defined as those with $D_{1\text{-}4}$ values exceeding 0.0015 $\mu m^2/s$), we observed distinct diffusion profiles derived from mean square displacement (MSD) plots (Figure V) (Manzo & García-Parajo Rep. Prog. Phys., 2015), which were further classified based on motion, using the moment scaling spectrum (MSS) (Ewers et al. PNAS, 2005). Under all experimental conditions, the majority of mobile particles, ~85%, showed confined

diffusion: for example under basal conditions, without ligand addition, ~90% of mobile particles showed confined diffusion, ~8.5% showed Brownian-free diffusion and ~1.5% exhibited directed motion (new Supplementary Figure 5A in the main manuscript). These data have been also included in the revised manuscript to show, in detail, the dynamic parameters of CXCR4.

Due to the space constraints, it is very difficult to include all the figures generated. However, to ensure comprehensive assessment and transparency (for the purpose of this review), we have included below representative plots of the MSD values as a function of time from individual trajectories, showing different types of motion obtained in our experiments (Author response image 4).

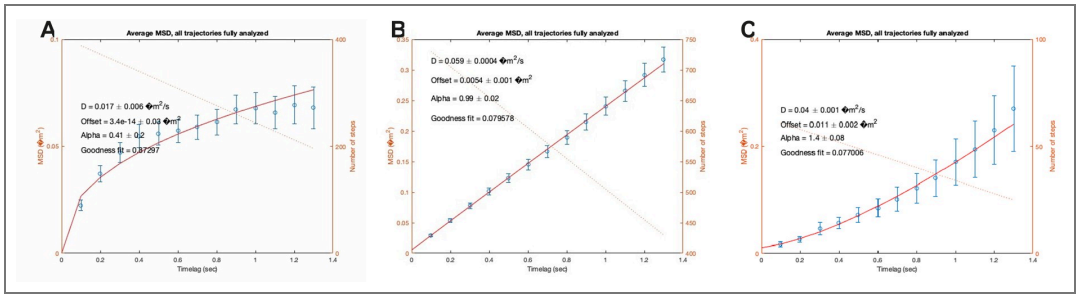


**Author response image 4. Representative MSD plots from individual trajectories of CXCR4AcGFP detected by SPT-TIRF in resting JKCD4 cells showing different types of motion: A) confined, B) Brownian/Free, C) direct transport.**

> *(4) Fig 1C,D - It would be helpful to see a plot of D vs MSI at a single particle level. In comparing C and D I'm surprised there is not a larger difference between CXCL12 and X4-gp120. It would also be very important to see the behaviour of X4-gp120 on the CXCR4 deficient Jurkat that would provide a picture of CD4 diffusion. The CXCR4 nanoclustering related to the X4-gp120 could be dominated by CD4 behaviour.*

As previously described, all analyses were performed under SPT conditions (see previous response to point 1). Figure 1C details the percentage of oligomers (>3 receptors/particle) calibrated using Jurkat $CD4^+$ cells electroporated with monomeric CD86-AcGFP (Dorsch et al. Nat. Methods, 2009). The monomer value was determined by analyzing photobleaching steps as described in our previous response to point 1.

In our experiments, we observed a trend towards a higher number of oligomers upon activation with CXCL12 compared with X4-gp120. This trend was further supported by measurements of Mean Spot Intensity. However, the values are also influenced by the number of larger spots, which represents a minor fraction of the total spots detected.

The differences between the effect triggered by CXCL12 or X4-gp120 might also be attributed to a combination of factors related to differences in ligand concentration, their structure, and even to the technical requirements of TIRF-M. Both ligands are in contact with the substrate (fibronectin) and the specific nature of this interaction may differ between both ligands and influence their accessibility to CXCR4. Moreover, the requirement of the prior binding of gp120 to CD4 before CXCR4 engagement, in contrast to the direct binding of CXCL12 to CXCR4, might also contribute to the differences observed.

We previously reported that CXCL12-mediated CXCR4 dynamics are modulated by CD4 coexpression (Martinez-Muñoz et al. Mol. Cell, 2018). We have now detected the formation of CD4 heterodimers with both CXCR4 and $CXCR4^{R334X}$, and found that these conformations are influenced by gp120-VLPs. In the present manuscript, we did not focus on CD4 clustering as it has been extensively characterized previously (Barrero-Villar et al. J. Cell Sci., 2009;

JiménezBaranda et al. Nat. Cell. Biol., 2007; Yuan et al. Viruses, 2021). Regarding the investigation of the effects of X4-gp120 on CXCR4-deficient Jurkat cells, which would provide a picture of CD4 diffusion, we would note that a previous report has already addressed this issue using single molecule super-resolution imaging, and revealed that CD4 molecules on the cell membrane are predominantly found as individual molecules or small clusters of up to 4 molecules, and that the size and number of these clusters increases upon virus binding or gp120 activation (Yuan et al. Viruses, 2021).

> *(5) Fig S1D- This data is really interesting. However, if both the CD4 and the gp120 have his tags they need to be careful as poly-His tags can bind weakly to cells and increasing valency could generate some background. So, they should make the control is fair here. Ideally, using non-his tagged person of sCD4 and gp120 would be needed ideal or they need a His-tagged Fab binding to gp120 that doesn't induce CXCR4 binding.*

New Supplementary Figure 2D shows that X4-gp120 does not bind Daudi cells (these cells do not express CD4) in the absence of soluble CD4. While the reviewer is correct to state that both proteins contain a Histidine Tag, cell binding is only detected if X4-gp120 binds sCD4. Nonetheless, we have included in the revised Supplementary Figure 2D a control showing the negative binding of sCD4 to Daudi cells in the absence of X4-gp120. Altogether, these results confirm that only sCD4/X4-gp120 complexes bind these cells.

> *(6) Fig S4- Panel D needs a scale bar. I can't figure out what I'm being shown without this.*

Apologies. A scale bar has been included in this panel (new Supplementary Figure 6D).

> ***Reviewer #2:***
>
> *(1) This study is well described in both the main text and figures. Introduction provides adequate background and cites the literature appropriately. Materials and Methods are detailed. Authors are careful in their interpretations, statistical comparisons, and include necessary controls in each experiment. The Discussion presents a reasonable interpretation of the results. Overall, there are no major weaknesses with this manuscript.*

We very much appreciate the positive comments of the reviewer regarding the broad interest and strength of our work.

> *(2) NL4-3deltaIN and immature HIV virions are found to have less associated gp120 relative to wild-type particles. It is not obvious why this is the case for the deltaIN particles or genetically immature particles. Can the authors provide possible explanations? (A prior paper was cited, Chojnacki et al Science, 2012 but can the current authors provide their own interpretation.)*

Our conclusion from the data is actually exactly the opposite. As shown in Figure 2D, the gp120 staining intensity was higher for NL4-3DIN particles (1,786 a.u.) than for gp120-VLPs (1,223 a.u.), indicating lower expression of Env proteins in the latter. Furthermore, analysis of gp120 intensity per particle (Figure 2E) confirmed that gp120-VLPs contained fewer gp120 molecules per particle than NL4-3DIN virions. These levels were comparable with, or even lower than, those observed in primary HIV-1 viruses (Zhu et al. Nature, 2006). This reduction was a direct consequence of the method used to generate the VLPs, as our goal was to produce viral particles with minimal gp120 content to prevent artifacts in receptor clustering that might occur using high levels of Env proteins in the VLPs to activate the receptors.

This misunderstanding may arise from the fact that we also compared Gag condensation and Env distribution on the surface of gp120-VLPs with those observed in genetically immature particles and integrase-defective NL4-3ΔIN virions, which served as controls. STED

microscopy data revealed differences in Env distribution between gp120-VLPs and NL4-3ΔIN virions, supporting the classification of gp120-VLPs as mature particles (Figure 2 A,B).

> ***Reviewer #3***:

We thank the reviewer for considering that our work offers new insights into the spatial organization of receptors during HIV-1 entry and infection and that the manuscript is well written, and the findings significant.

> *(1) For mechanistic basis of gp120-CXCR4 versus CXCL12-CXCR4 differences. Provide additional structural or biochemical evidence to support the claim that gp120 stabilises a distinct CXCR4 conformation compared to CXCL12. If feasible, include molecular modelling, mutagenesis, or crosslinking experiments to corroborate the proposed conformational differences.*

We appreciate the opportunity to clarify this point. The specific claim that gp120 stabilizes a conformation of CXCR4 that is distinct from the CXCL12-bound state was not explicitly stated in our manuscript, although we agree that our data strongly support this possibility. It is important to consider that CXCL12 binds directly to CXCR4, whereas gp120 requires prior sequential binding to CD4, and its subsequent interaction is with a CXCR4 molecule that is already forming part of the CD4/CXCR4 complex, as demonstrated by our FRET experiments and supported by previous studies (Zaitseva et al. J. Leuk. Biol., 2005; Busillo & Benovic Biochim. Biophys. Acta, 2007; Martínez-Muñoz et al. PNAS, 2014). This difference makes it inherently complex to compare the conformational changes induced by gp120 and CXCL12 on CXCR4.

However, our findings show that both stimuli induce oligomerization of CXCR4, a phenomenon not observed when mutant $CXCR4^{R334X}$ was exposed to the chemokine CXCL12 (García-Cuesta et al. PNAS, 2022).

(1) CXCL12 induced oligomerization of CXCR4 but did not affect the dynamics of $CXCR4^{R334X}$ (Martinez-Muñoz et al. Mol. Cell, 2018; García-Cuesta et al. PNAS, 2022). By contrast, X4-gp120 and the corresponding VLPs—which require initial binding to CD4 to engage the chemokine receptor—stabilized oligomers of both CXCR4 and $CXCR4^{R334X}$.

(2) FRET analysis revealed distinct $FRET_{50}$ values for CD4/CXCR4 (2.713) and CD4/$CXCR4^{R334X}$ (0.399) complexes, suggesting different conformations for each complex.

(3) Consistent with previous reports (Balabanian et al. Blood, 2005; Zmajkovicova et al. Front. Immunol., 2024; García-Cuesta et al. PNAS, 2022), the molecular mechanisms activated by CXCL12 are distinct when comparing CXCR4 with $CXCR4^{R334X}$. For instance, CXCL12 induces internalization of CXCR4, but not of mutant $CXCR4^{R334X}$. Conversely, X4-gp120 triggers approximately 25% internalization of both receptors. Similarly, CXCL12 does not promote CD4 internalization in cells co-expressing CXCR4 or $CXCR4^{R334X}$, whereas X4-gp120 does, although CD4 internalization was significantly higher in cells co-expressing CXCR4.

These findings suggest that CD4 influences the conformation and the oligomerization state of both co-receptors. To further support this hypothesis, we have conducted new in silico molecular modeling of CD4 in complex with either CXCR4 or its mutant $CXCR4^{R334X}$ using AlphaFold 3.0 (Abramson et al. Nature, 2024). The server was provided with both sequences, and the interaction between the two molecules for each protein was requested. It produced a number of solutions, which were then analyzed using the software ChimeraX 1.10 (Meng et al. Protein Sci., 2023). CXCR4 and its mutant, $CXCR4^{R334X}$ bound to CD4, were superposed using one of the CD4 molecules from each complex, with the aim of comparing the spatial positioning of CD4 molecules when interacting with CXCR4.

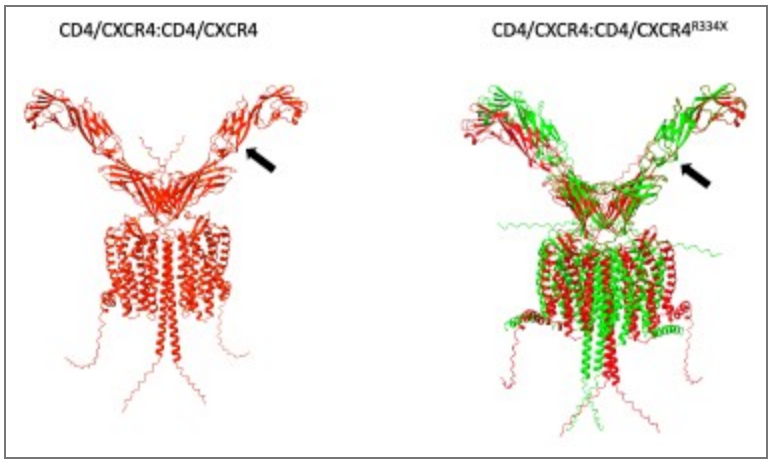


**Author response image 5. CD4/CXCR4 complexes were superimposed with CD4/CXCR4 complexes (left panel) or CD4/CXCR4$^{R334X}$ complexes (right panels).** Arrows indicate the CD4 molecule used as reference for the superimposing.

As illustrated in Author response image 5, the superposition of the CD4/CXCR4 complexes was complete. However, when CD4/CXCR4 complexes were superimposed with CD4/CXCR4$^{R334X}$ complexes using the same CD4 molecule as a reference, indicated by an arrow in the figure, a clear structural deviation became evident. The main structural difference detected was the positioning of the CD4 transmembrane domains when interacting with either the wild-type or mutant CXCR4. While in complexes with CXCR4, the angle formed by the lines connecting residues E416 at the C-terminus end of CD4 with N196 in CXCR4 was 12°, for the CXCR4$^{R334X}$ complex, this angle increased to 24°, resulting in a distinct orientation of the CD4 extracellular domain (Author response image 6).

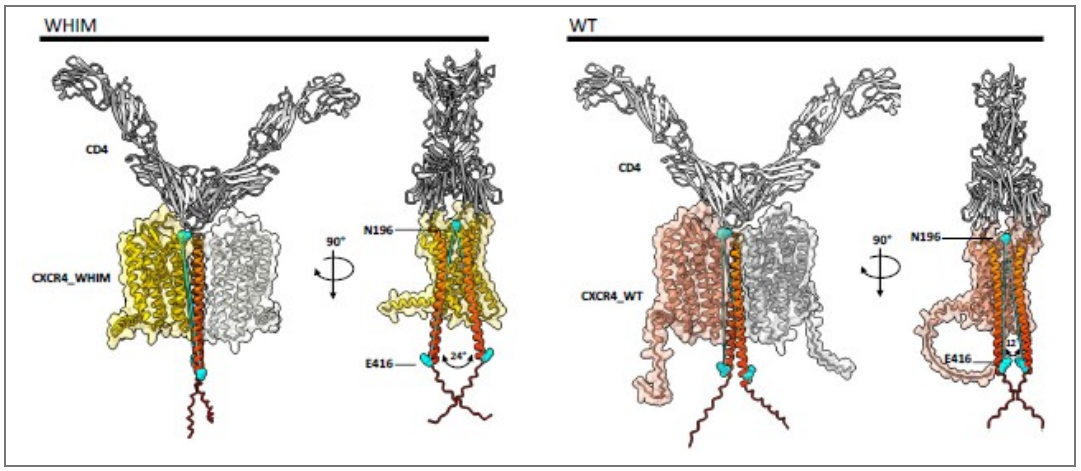


**Author response image 6. Comparison of the angle between the transmembrane domains of CD4 in CXCR4 WT and WHIM complexes.** The angle between residues N196 from one CXCR4 molecule and E416 from the two CD4 dimer molecules was calculated for the CXCR4 WT (12°) and WHIM (24°) complexes to demonstrate the difference in CD4 positioning.

To further analyze the models obtained, we employed PDBsum software (Laskowski & Thornton Protein Sci., 2021) to predict the CD4/CXCR4 interface residues. Data indicated that at least 50% of the interaction residues differed when the CD4/CXCR4 interaction surface was compared with that of the CD4/CXCR4$^{R334X}$ complex (Author response image 7). It is important to note that while some hydrogen bonds were present in both complex models, others were exclusive to one of them. For instance, whereas Cys$^{394}$(CD4)-Tyr$^{139}$ and

Lys$^{299}$(CD4)-Glu$^{272}$ were present in both CD4/CXCR4 and CD4/CXCR4$^{R334X}$ complexes, the pairs Asn$^{337}$(CD4)-Ser$^{27}$(CXCR4$^{R334X}$) and Lys$^{325}$(CD4)-Asp$^{26}$(CXCR4$^{R334X}$) were only found in CD4/CXCR4$^{R334X}$ complexes.

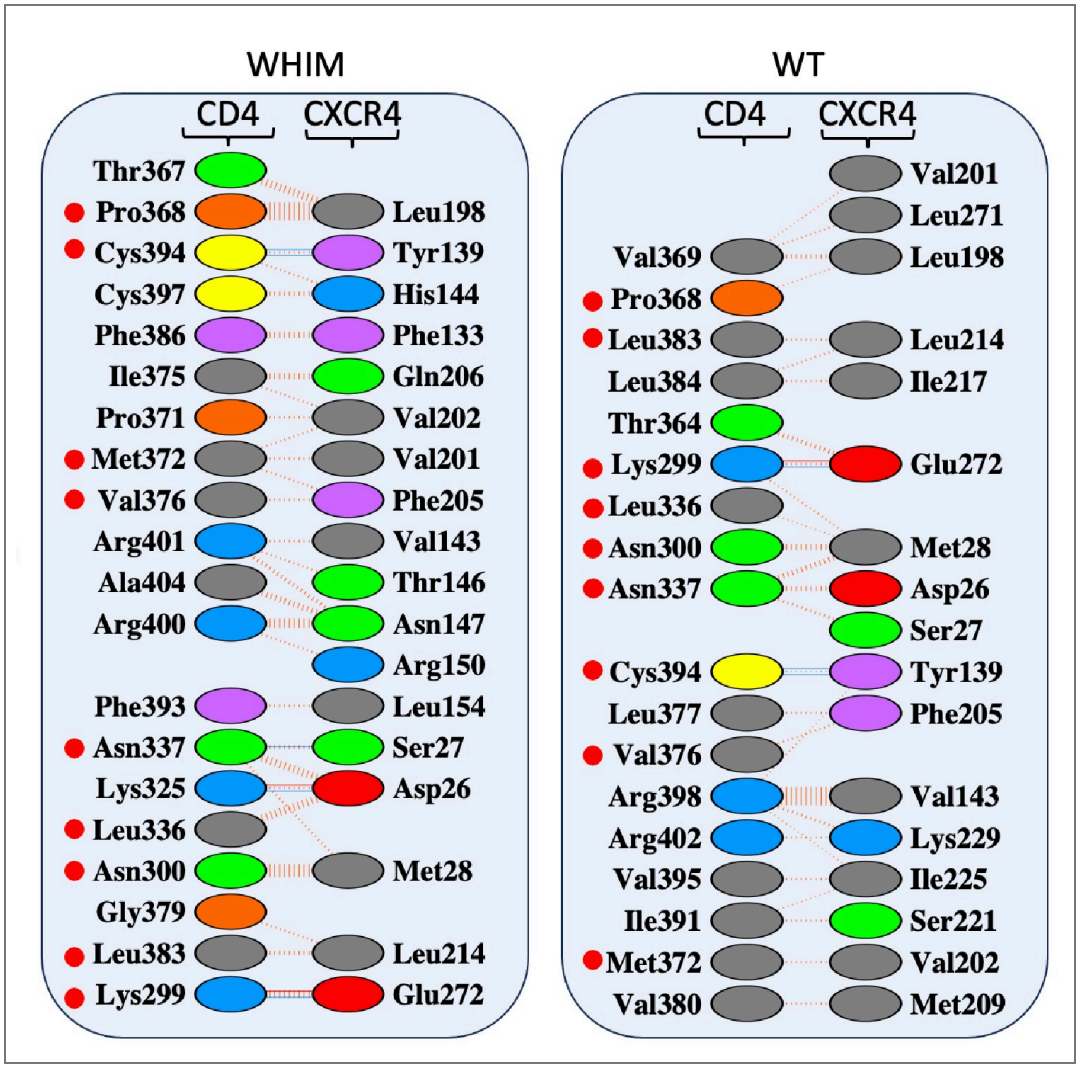


**Author response image 7. Interacting residues at the CD4/CXCR4 interface.** The panel displays the interface residues from the CXCR4 and CD4 oligomer. CD4 residues labeled with a red sphere show the interacting residues present in both CXCR4-WT and –WHIM hetero- oligomers. The continuous red lines represent a saline bridge, while the blue lines indicate a hydrogen bond and the dashed red lines represent non-bonded interactions. As illustrated in the figure, half of the interacting residues differ between the WT and WHIM models, indicating that the interacting surfaces are also distinct.

These findings, which are consistent with our FRET results, suggest distinct interaction surfaces between CD4 and the two chemokine receptors. Overall, these results are compatible with differences in the spatial conformation adopted by these complexes.

> *(2) For Empty VLP effects on CXCR4 dynamics: Explore potential causes for the observed effects of Envdeficient VLPs. It's valuable to include additional controls such as particles from non-producer cells, lipid composition analysis, or blocking experiments to assess nonspecific interactions.*

As VLPs are complex entities, we thought that the relevant results should be obtained comparing the effects of Env(-) VLPs with gp120-VLPs. Therefore, we would first remark that

regardless of the effect of Env(-) VLPs on CXCR4 dynamics, the most evident finding in this study is the strong effect of gp120-VLPs compared with control Env(-) VLPs. Nevertheless, regarding the effect of the Env(-) VLPs compared with medium, we propose several hypotheses. As several virions can be tethered to the cell surface via glycosaminoglycans (GAGs), we hypothesized that VLPs-GAGs interactions might indirectly influence the dynamics of CXCR4 and CXCR4$^{R334X}$ at the plasma membrane. Additionally, membrane fluidity is essential for receptor dynamics, therefore VLPs interactions with proteins, lipids or any other component of the cell membrane could also alter receptor behavior. It is well known that lipid rafts participate in the interaction of different viruses with target cells (Nayak & Hu Subcell. Biochem., 2004; Manes et al. Nat. Rev. Immunol., 2003; Rioethmullwer et al. Biochim. Biophys. Acta, 2006) and both the lipid composition and the presence of co-expressed proteins modulate ligand-mediated receptor oligomerization (Gardeta et al. Frontiers in Immunol., 2022; Gardeta et al. Cell. Commun. Signal., 2025). We have thus performed Raster Image Correlation Spectroscopy (RICS) analysis to assess membrane fluidity through membrane diffusion measurements on cells treated with Env(-) VLPs.

Jurkat cells were labeled with Di-4-ANEPPDHG and seeded on FN and on FN + VLPs prior to analysis by RICS on confocal microscopy. The results indicated no significant differences in membrane diffusion under the treatment tested, thereby discarding an effect of VLPs on overall membrane fluidity (Author response image 8).

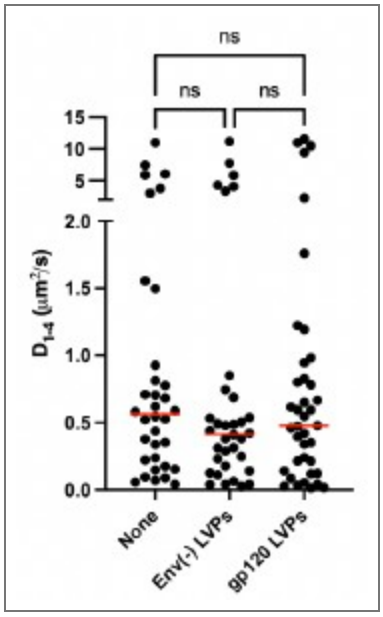


**Author response image 8. VLPs treatment does not alter cell membrane fluidity.** Diffusion values obtained by RICS from JKCD4X4 cells. (n = 3, with at least 10 cells analyzed per experiment and condition; n.s., not significant).

Nonetheless, these results do not rule out other non-specific interactions of Env(-) VLPs with membrane proteins that could affect receptor dynamics. For instance, it has been reported that Ctype lectin DC-SIGN acts as an efficient docking site for HIV-1 (Cambi et al. J. Cell. Biol., 2004; Wu & KewalRamani Nat. Rev. Immunol., 2006). However, a detailed investigation of these possible mechanisms is beyond the scope of this manuscript.

> *(3) For Direct link between clustering and infection efficiency - Test whether disruption of CXCR4 clustering (e.g., using actin cytoskeleton inhibitors, membrane lipid perturbants, or clustering-deficient mutants) alters HIV-1 fusion or infection efficiency.*

Designing experiments using tools that disrupt receptor clustering by interacting with the receptors themselves is difficult and challenging, as these tools bind the receptor and can

therefore alter parameters such as its conformation and/or its distribution at the cell membrane, as well as affect some cellular processes such as HIV-1 attachment and cell entry. Moreover, effects on actin polymerization or lipids dynamics can affect not only receptor clustering but also impact on other molecular mechanisms essential for efficient infection.

Many previous reports have, nonetheless, indirectly correlated receptor clustering with cell infection efficiency. Cholesterol plays a key role in the entry of several viruses. Its depletion in primary cells and cell lines has been shown to confer strong resistance to HIV-1-mediated syncytium formation and infection by both CXCR4- and CCR5-tropic viruses (Liao et al. AIDS Res. Hum. Retroviruses, 2021). Moderate cholesterol depletion also reduces CXCL12-induced CXCR4 oligomerization and alters receptor dynamics (Gardeta et al. Cell. Commun. Signal., 2025). By restricting the lateral diffusion of CD4, sphingomyelinase treatment inhibits HIV-1 fusion (Finnegan et al. J. Virol., 2007). Depletion of sphingomyelins also disrupts CXCL12mediated CXCR4 oligomerization and its lateral diffusion (Gardeta et al. Front Immunol., 2022). Additional reports highlight the role of actin polymerization at the viral entry site, which facilitates clustering of HIV-1 receptors, a crucial step for membrane fusion (Serrano et al. Biol. Cell., 2023). Blockade of actin dynamics by Latrunculin A treatment, a drug that sequesters actin monomers and prevents its polymerization, blocks CXCL12-induced CXCR4 dynamics and oligomerization (Martínez-Muñoz et al. Mol. Cell, 2018).

Altogether, these findings strongly support our hypothesis of a direct link between CXCR4 clustering and the efficiency of HIV-1 infection.

> *(4) CD4/CXCR4 co-endocytosis hypothesis - Support the proposed model with direct evidence from livecell imaging or co-localization experiments during viral entry. Clarification is needed on whether internalization is simultaneous or sequential for CD4 and CXCR4.*

When referring to endocytosis of CD4 and CXCR4, we only hypothesized that HIV-1 might promote the internalization of both receptors either sequentially or simultaneously. The hypothesis was based in several findings:

a) Previous studies have suggested that HIV-1 glycoproteins can reduce CD4 and CXCR4 levels during HIV-1 entry (Choi et al. Virol. J., 2008; Geleziunas et al. FASEB J, 1994; Hubert et al. Eur. J. Immunol., 1995).

b) Receptor endocytosis has been proposed as a mechanism for HIV-1 entry (Daecke et al. J. Virol., 2005; Aggarwal et al. Traffick, 2017; Miyauchi et al. Cell, 2009; Carter et al. Virology, 2011).

c) Our data from cells activated with X4-gp120 demonstrated internalization of CD4 and chemokine receptors, which correlated with HIV-1 infection in PBMCs from WHIM patients and healthy donors.

d) CD4 and CXCR4 have been shown to co-localize in lipid rafts during HIV-1 infection (Manes et al. EMBO Rep., 2000; Popik et al. J. Virol., 2002)

e) Our FRET data demonstrated that CD4 and CXCR4 form heterocomplexes and that FRET efficiency increased after gp120-VLPs treatment.

We agree with the reviewer that further experiments are required to test this hypothesis, however, we believe that this is beyond the scope of the current manuscript.

> *Minor Comments:*

> *(1) The conclusions rely solely on the HXB2 X4-tropic Env. It would strengthen the study to assess whether other X4 or dual-tropic strains induce similar receptor clustering and dynamics.*

The primary goal of our current study was to investigate the dynamics of the co-receptor CXCR4 during HIV-1 infection, motivated by previous reports showing CD4 oligomerization upon HIV1 binding and gp120 stimulation (Yuan et al. Viruses, 2021). We initially used a recombinant X4gp120, a soluble protein that does not fully replicate the functional properties of the native HIV-1 Env. Previous studies have shown that Env consists of gp120 trimers, which redistribute and cluster on the surface of virions following proteolytic Gag cleavage during maturation (Chojnacki et al. Nat. Commun., 2017). An important consideration in receptor oligomerization studies is the concentration of recombinant gp120 used, as it does not accurately reflect the low number of Env trimers present on native HIV-1 particles (Hart et al. J. Histochem. Cytochem., 1993; Zhu et al. Nature, 2006). To address these limitations, we generated virus-like particles (VLPs) containing low levels of X4-gp120 and repeated the dynamic analysis of CXCR4. The use of primary HIV-1 isolates was limited, in this project, to confirm that PBMCs from both healthy donors and WHIM patients were equally susceptible to infection. This result using a primary HIV-1 virus supports the conclusion drawn from our *in vitro* approaches. We thus believe that although the use of other X4- and dual-tropic strains may complement and reinforce the analysis, it is far beyond the scope of the current manuscript.

> *(2) Given the observed clustering effects, it would be valuable to explore whether gp120-induced rearrangements alter epitope exposure to broadly neutralizing antibodies like 17b or 3BNC117. This would help connect the mechanistic insights to therapeutic relevance.*

As 3BNC117, VRC01 and b12 are broadly neutralizing mAbs that recognize conformational epitopes on gp120 (Li et al. J. Virol., 2011; Mata-Fink et al. J. Mol. Biol., 2013), they will struggle to bind the gp120/CD4/CXCR4 complex and therefore may not be ideal for detecting changes within the CD4/CXCR4 complex. The experiment suggested by the reviewer is thus challenging but also very complex. It would require evaluating antibody binding in two experimental conditions, in the absence and in the presence of oligomers. However, our data indicate that receptor oligomerization is promoted by X4-gp120 binding, and the selected antibodies are neutralizing mAbs, so they should block or hinder the binding of gp120 and, consequently, receptor oligomerization. An alternative approach would be to study the neutralizing capacity of these mAbs on cells expressing CD4/CXCR4 or CD4/CXCR4$^{R334X}$ complexes. Variations in their neutralizing activity could be then extrapolated to distinct gp120 conformations, which in turn may reflect differences between CD4/CXCR4 and CD4/CXCR4$^{R334X}$ complexes.

We thus assessed the ability of the VRC01 and b12, anti-gp120 mAbs, which were available in our laboratory, to neutralize gp120 binding on cells expressing CD4/CXCR4 or CD4/CXCR4$^{R334X}$. Specifically, increasing concentrations of each antibody were preincubated (60 min, 37ºC) with a fixed amount of X4-gp120 (0.05 μg/ml). The resulting complexes were then incubated with Jurkat cells expressing CD4/CXCR4 or CD4/CXCR4$^{R334X}$ (30 min, 37ºC) and, finally, their binding was analyzed by flow cytometry. Although we did not observe statistically significant differences in the neutralization capacity of b12 or VRC01 for the binding of X4-gp120 depending on the presence of CXCR4 or CXCR4$^{334X}$, we observed a trend for greater concentrations of both mAbs to neutralize X4-gp120 binding in Jurkat CD4/CXCR4 cells than in Jurkat CD4/CXCR4$^{R334X}$ cells (Author response image 9).

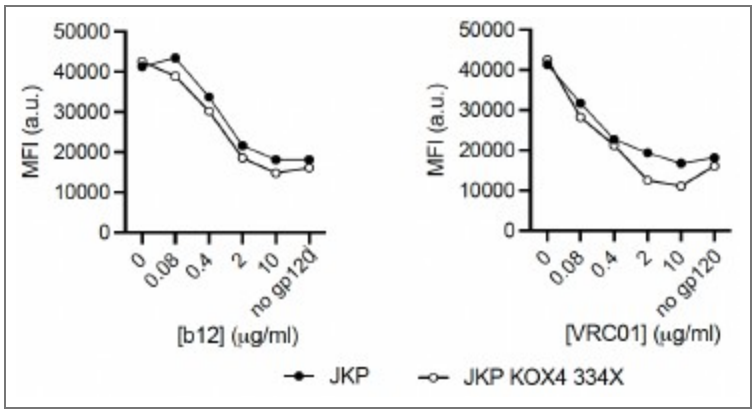


**Author response image 9. Flow cytometry analysis of gp120 binding to Jurkat cells expressing CD4/CXCR4 or CD4/CXCR4$^{R334X}$ in the presence of different concentrations of the neutralizing anti-gp120 antibodies b12 (left panel) and VRC01 (right panel).** AUC comparison by Welch's t-test: pvalues 0.2950 and 0.2112 for b12 and VRC01 respectively (n = 2).

These slight alterations in the neutralizing capacity of b12 and VRC01 mAbs may thus suggest minimal differences in the conformations of gp120 depending of the coreceptor used. We also detected that X4-gp120 and VLPs expressing gp120, which require initial binding to CD4 to engage the chemokine receptor, stabilized oligomers of both CXCR4 and CXCR4$^{R334X}$, but FRET data indicated distinct $FRET_{50}$ values between the partners, (2.713) for CD4/CXCR4 and (0.399) for CD4/CXCR4$^{R334X}$ (Figure 5A,B in the main manuscript). Moreover, we also detected significantly more CD4 internalization mediated by X4-gp120 in cells co-expressing CD4 and CXCR4 than in those co-expressing CD4 and CXCR4$^{R334X}$ (Figure 6 in the main manuscript). Overall these latter data and those included in Author response images 5,6 and 7 indicate distinct conformations within each receptor complexes.

> *(3) TIRF imaging limits analysis to the cell substrate interface. It would be useful to clarify whether CXCR4 receptor clustering occurs elsewhere, such as at immunological synapses or during cell-to-cell contact.*

In recent years, chemokine receptor oligomerization has gained significant research interest due to its role in modulating the ability of cells to sense chemoattractant gradients. This molecular organization is now recognized as a critical factor in governing directed cell migration (Martínez-Muñoz et al. Mol. Cell, 2018; García-Cuesta et al. PNAS, 2022, Hauser et al. Immunity, 2016). In addition, advanced imaging techniques such as single-molecule and super-resolution microscopy have been used to investigate the spatial distribution and dynamic behaviour of CXCR4 within the immunological synapse in T cells (Felce et al. Front. Cell Dev. Biol., 2020). Building on these findings, we are currently conducting a project focused on characterizing CXCR4 clustering specifically within this specialized cellular region.

> *(4) In LVP experiments, it would be useful to report transduction efficiency (% GFP+ cells) alongside MSI data to relate VLP infectivity with receptor clustering functionally.*

These experiments were designed to validate the functional integrity of the gp120 conformation on the LVPs, confirming their suitability for subsequent TIRF microscopy. Our objective was to establish a robust experimental tool rather than to perform a high-throughput quantification of transduction efficiency. It is for that reason that these experiments were included in new Supplementary Figure S6, which also contains the complete characterization of gp120-VLPs and LVPs. In such experimental conditions, quantifying the percentage of GFP-positive cells relative to the total number of cells plated in each well is very difficult. However, in line with the reviewer's commentary and as we used the same number of cells in each experimental condition, we have included, in the revised

manuscript, a complementary graph illustrating the GFP intensity (arbitrary units) detected in all the wells analyzed (new Supplementary Fig. 6E).

> *(5) To ensure that differences in fusion events (Figure 7B) are attributable to target cell receptor properties, consider confirming that effector cells express similar levels of HIV-1 Env. Quantifying gp120 expression by flow cytometry or western blot would rule out the confounding effects of variable Env surface density.*

In these assays (Figure 7B), we used the same effector cells (cells expressing X4-gp120) in both experimental conditions, ensuring that any observed differences should be attributable solely to the target cells, either JKCD4X4 or JKCD4X4$^{R334X}$. For this reason, in Figure 7A we included only the binding of X4-gp120 to the target cells which demonstrated similar levels of the receptors expressed by the cells.

> *(6) HIV-mediated receptor downregulation may occur more slowly than ligand-induced internalization. Including a 24-hour time point would help assess whether gp120 induces delayed CD4 or CXCR4 loss beyond the early effects shown and to better capture potential delayed downregulation induced by gp120.*

The reviewer suggests using a 24-hour time point to facilitate detection of receptor internalization. However, such an extended incubation time may introduce some confounding factors, including receptor degradation, recycling and even de novo synthesis, which could affect the interpretation of the results. Under our experimental conditions, we observed that CXCL12 did not trigger CD4 internalization whereas X4-gp120 did. Interestingly, CD4 internalization depended on the coreceptor expressed by the cells.

> *(7) Increase label font size in microscopy panels for improved readability.*

Of course; the font size of these panels has been increased in the revised version.

> *(8) Consider adding more references on ligand-induced co-endocytosis of CD4 and chemokine receptors during HIV-1 entry.*

We have added more references to support this hypothesis (Toyoda et al. J. Virol., 2015; Venzke et al. J. Virol., 2006; Gobeil et al J. Virol., 2013).

> *(9) For Statistical analysis. Biological replicates are adequate, and statistical tests are generally appropriate. For transparency, report n values, exact p-values, and the statistical test used in every figure legend and discussed in the results.*

Thank you for highlighting the importance of transparency in statistical reporting. We confirm that the n values for all experiments have been included in the figure legends. The statistical tests used for each analysis are also clearly indicated in the figure legends, and the interpretation of these results is discussed in detail in the Results section. Furthermore, the Methods section specifies the tests applied and the thresholds for significance, ensuring full transparency regarding our analytical approach.

In accordance with established conventions in the field, we have utilized categorical significance indicators (e.g., n.s., *, **, ***) within our figures to enhance readability and focus on biological trends. This approach is widely adopted in high-impact literature to prevent visual clutter. However, to ensure full transparency and reproducibility, we have ensured that the underlying statistical tests and thresholds are clearly defined in the respective figure legends and Methods section.

> ***Reviewer #4:***

We thank the reviewer for considering that this work is presented in a clear fashion, and the main findings are properly highlighted, and for remarking that the paper is of interest to the

retrovirology community and possibly to the broader virology community.

We also agree on the interest that X4-gp120 clusters $CXCR4^{R334X}$ suggests a different binding mechanism for X4-gp120 from that of the natural ligand CXCL12, an aspect that we are now evaluating. These data also indicate that WHIM patients can be infected by HIV-1 similarly to healthy people.

> *(1) The observation that "empty VLPs" reduce CXCR4 diffusivity is potentially interesting. However, it is not supported by the data owing to insufficient controls. The authors correctly discuss the limitations of that observation in the Discussion section (lines 702-704). However, they overinterpret the observation in the Results section (lines 509-512), suggesting non-specific interactions between empty VLPs, CD4 and CXCR4. I suggest either removing the sentence from the Results section or replacing it with a sentence similar to the one in the Discussion section.*

In accordance with the reviewerṡ suggestion, the sentence in the result section has been replaced with one similar to that found in the discussion section. In addition, we have performed Raster Image Correlation Spectroscopy (RICS) analysis using the Di-4-ANEPPDHQ lipid probe to assess membrane fluidity by means of membrane diffusion, and compared the results with those of cells treated with Env(-) VLPs. The results indicated that VLPs did not modulate membrane fluidity (Author response image 8). Nonetheless, these results do not rule out other potential non-specific interactions of the Env(-) VLPs with other components of the cell membrane that might affect receptor dynamics (see our response to point 2 of reviewer #3).

> *(2) In the case of the WHIM mutant CXCR4-R334X, the addition of "empty VLPs" did not cause a significant change in the diffusivity of CXCR4-R334X (Figure 4B). This result is in contrast with the addition of empty VLPs to WT CXCR4. However, the authors neither mention nor comment on that result in the results section. Please mention the result in the paper and comment on it in relation to the addition of empty VLPs to WT CXCR4.*

We would remark that the main observation in these experiments should focus on the effect of gp120-VLPs, and the results indicates that gp120-VLPs promoted clustering of CXCR4 and of $CXCR4^{R334X}$ and reduced their diffusion at the cell membrane. The Env(- ) VLPs were included as a negative control in the experiments, to compare the data with those obtained using gp120VLPs. However, once we observed some residual effect of the Env(-) VLPs, we decided to give a potential explanation, formulated as a hypothesis, that the Env(-) VLPs modulated membrane fluidity. We have now performed a RICS analysis using Di-4-ANEPPDHQ as a lipid probe (Author response image 9). The results suggest that Env(-) VLPs do not modulate cell membrane fluidity, although we do not rule out other potential interactions with membrane proteins that might alter receptor dynamics. We appreciate the reviewer's observation and agree that this result can be noted. However, since the main purpose of Figure 4B is to show that gp120-VLPs modulate the dynamics of $CXCR4^{R334X}$ rather than to remark that the Env(-) VLPs also have some effects, we consider that a detailed discussion of this specific aspect would detract from the central finding and may dilute the primary narrative of the study.

> *Minor comments*
>
> *(1) It would be helpful for the reader to combine thematically or experimentally linked figures, e.g., Figures 3 and 4.*
>
> *(2) Figures 3 and 4 are very similar. Please unify the colours in them and the order of the panels (e.g. Figure 3 panel A shows diffusivity of CXCR4, while Figure 4 panel A shows MSI of CXCR4-R334X).*

While we considered consolidating Figures 3 and 4, we believe that maintaining them as separate entities enhances conceptual clarity. Since Figure 3 establishes the baseline

dynamics for wildtype CXCR4 and Figure 4 details the distinct behavior of the CXCR4$^{R334X}$ mutant, keeping them separate allows the reader to fully appreciate the specificities of each system before making a cross-comparison.

> *(3) Some parts of the Discussion section could be shortened, moved to the Introduction (e.g., lines 648651), or entirely removed (e.g., lines 633-635 about GPCRs).*

In accordance, the Discussion section has been reorganized and shortened to improve clarity.

> *(4) I suggest renaming "empty VLPs" to "Env(−) VLPs" (or similar). The name empty VLPs can mislead the reader into thinking that these are empty vesicles.*

The term empty VLPs has been renamed to Env(−) VLPs throughout the manuscript to more accurately reflect their composition. Many thanks for this suggestion.

> *(5) Line 492 - please rephrase "...lower expression of Env..." to "...lower expression of Env or its incorporation into the VLPs...".*

The sentence has been rephrased

> *(6) Line 527 - The data on CXCL12 modulating CXCR4-R334X dynamics and clustering are not present in Figure 4 (or any other Figure). Please add them or rephrase the sentence with an appropriate reference. Make clear which results are yours.*
>
> *(7) Line 532 - Do the data in the paper really support a model in which CXCL12 binds to CXCR4R334X? If not, please rephrase with an appropriate reference.*

Previous studies support the association of CXCL12 with CXCR4$^{R334X}$ (Balabanian et al. Blood, 2005; Hernandez et al. Nat Genet., 2003; Busillo & Benovic Biochim. Biophys. Acta, 2007). In fact, this receptor has been characterized as a gain-of-function variant for this ligand (McDermott et al. J. Cell. Mol. Med., 2011). The revised manuscript now includes these bibliographic references to support this commentary. In any case, our previous data indicate that CXCL12 binding does not affect CXCR4$^{R334X}$ dynamics (García-Cuesta et al. PNAS, 2022).

> *(8) Line 695 - "...lipid rafts during HIV-1 (missing word?) and their ability to..." During what?*

Many thanks for catching this mistake. The sentence now reads: “Although direct evidence for the internalization of CD4 and CXCR4 as complexes is lacking, their co-localization in lipid rafts during HIV-1 infection (97–99) and their ability to form heterocomplexes (22) strongly suggest they could be endocytosed together.”

https://doi.org/10.7554/eLife.110354.1.sa0